Neurobiology of Disease

Rare GPR37L1 Variants Reveal Potential Association between GPR37L1 and Disorders of Anxiety and Migraine

Gerda E. Breitwieser,[1] Andrea Cippitelli,[1] Yingcai Wang,[1] Oliver Pelletier,[1] Ridge Dershem,[1] Jianning Wei,[1] Lawrence Toll,[1] Bianca Fakhoury,[1] Gloria Brunori,[1] Raghu Metpally,[2] David J. Carey,[3] the Regeneron Genetics Center[4] and Janet Robishaw[1,5]

[1]Charles E. Schmidt College of Medicine, Florida Atlantic University, Boca Raton, Florida, [2]Sonic Healthcare USA, Rye Brook, New York, [3]Geisinger, Weis Center for Research, Danville, Pennsylvania, [4]Regeneron Genetics Center, Tarrytown, New York, and [5]College of Veterinary Medicine, University of Florida, Gainesville, Florida

GPR37L1 is an orphan receptor that couples through heterotrimeric G-proteins to regulate physiological functions. Since its role in humans is not fully defined, we used an unbiased computational approach to assess the clinical significance of rare *G-protein-coupled receptor 37-like 1* (*GPR37L1*) genetic variants found among 51,289 whole-exome sequences from the DiscovEHR cohort. Rare *GPR37L1* coding variants were binned according to predicted pathogenicity and analyzed by sequence kernel association testing to reveal significant associations with disease diagnostic codes for epilepsy and migraine, among others. Since associations do not prove causality, rare *GPR37L1* variants were functionally analyzed in SK-N-MC cells to evaluate potential signaling differences and pathogenicity. Notably, receptor variants exhibited varying abilities to reduce cAMP levels, activate mitogen-activated protein kinase (MAPK) signaling, and/or upregulate receptor expression in response to the agonist prosaptide (TX14(A)), as compared with the wild-type receptor. In addition to signaling changes, knock-out (KO) of *GPR37L1* or expression of certain rare variants altered cellular cholesterol levels, which were also acutely regulated by administration of the agonist TX14(A) via activation of the MAPK pathway. Finally, to simulate the impact of rare nonsense variants found in the large patient cohort, a KO mouse line lacking *Gpr37l1* was generated. Although KO animals did not recapitulate an acute migraine phenotype, the loss of this receptor produced sex-specific changes in anxiety-related disorders often seen in chronic migraineurs. Collectively, these observations define the existence of rare *GPR37L1* variants associated with neuropsychiatric conditions in the human population and identify the signaling changes contributing to pathological processes.

Key words: **disease association; genetic variation; neurobiology; receptor; signal transduction**

Significance Statement

G-protein-coupled receptors represent a diverse group of membrane receptors that contribute to a wide range of diseases and serve as effective drug targets. However, a number of these receptors have no identified ligands or functions, that is, orphan receptors. Over the past decade, advances have been made, but there is a need for identifying new strategies to reveal their roles in health and disease. Our results highlight the utility of rare variant analyses of orphan receptors for identifying human disease associations, coupled with functional analyses in relevant cellular and animal systems, to ultimately reveal their roles as novel drug targets for treatment of neurological disorders that lack widespread efficacy.

Introduction

Migraine is a common neurovascular disorder affecting 12–15% of adults with a strong sex bias toward females (Burch et al., 2015; Bonafede et al., 2018). Migraine frequency and symptomology vary widely among individuals. Dissection of the underlying neurobiology has focused on increased neuronal hyperexcitability (Goadsby et al., 2017; Sutherland et al., 2019) and/or changes in the trigeminal–vascular system of the dura (Noseda and Burstein, 2013; Goadsby et al., 2017).

Received June 30, 2023; revised March 8, 2024; accepted March 11, 2024.

Author contributions: G.E.B., L.T., R.M., and J.R. designed research; A.C., Y.W., O.P., R.D., J.W., B.F., G.B., and R.M. performed research; D.J.C., R.G.C., and J.R. contributed unpublished reagents/analytic tools; G.E.B., A.C., O.P., R.D., J.W., B.F., G.B., R.M., and J.R. analyzed data; J.R. wrote the paper.

Funding of this work was supported in part by NIH R01GM111913 awarded to J.D.R. (MPI) and R01DA023281 to L.T. We thank Kirk Jeffreys for helping with initial experiments, Dr. Diane Smelser for helpful discussions, and Geisinger for support in early stages of these studies including access to the MyCode clinical and genomic data. We acknowledge and appreciate the generosity of the Geisinger patients who agreed to allow their data to be used for research.

Correspondence should be addressed to Janet Robishaw at robishawj@ufl.edu.

https://doi.org/10.1523/JNEUROSCI.1226-23.2024

The causal basis for susceptibility to migraine remains poorly understood. Genetic differences account for up to 60% of migraine occurrence (Russell et al., 1995; Mulder et al., 2003; Gormley et al., 2016; Hansen et al., 2017; Sutherland et al., 2019). At one end of the spectrum, genome-wide association studies (GWAS) and subsequent meta-analyses of migraine have identified common markers (single nucleotide polymorphisms, SNPs) in or near genes associated with glutamate signaling (*MTDH/AEG-1*, *LRP1*, *MEF2D*), synaptic development (*ASTN2*, *FHL5*), endothelial cell and blood vessel wall function (*PHACTR1*, *MMP16*, *AJAP1*, *TSPAN2*, *TGFBR2*), pain pathways (*TRPM8*), or metabolism (*PRDM16*, *C7orf10*) (Gormley et al., 2016). Since GWAS loci are commonly found in intronic or intergenic regions, assigning them to adjacent genes and defining pathologic mechanisms has been challenging. At the other end, familial studies have identified rare mutations in specific genes (*NOTCH3*, *TREX1*, *CACNA1A*, *ATP1A2*, *SCN1A*) associated with monogenic hemiplegic migraine (Hansen et al., 2017; Sutherland et al., 2019, 2020). Since rare variants are often present in coding regions, understanding how these mutations directly affect protein function and contribute to migraine is now emerging (Tardiolo et al., 2019). Although both strategies provide important mechanistic insights, the cumulative impact of known genes accounts for only a small fraction of estimated migraine heritability.

To address the "missing" heritability, recent attention has focused on the possible contribution of genes carrying rare variants that are not captured by GWAS genotyping assays and exert moderate effects not easily detected by classical linkage analysis in familial studies (Manolio et al., 2009). As a test of this concept, we selected 85 G-protein-coupled receptors (GPCRs) (Dershem et al., 2019) whose endogenous ligands, biological functions, and disease contributions have not been fully elucidated, that is, orphan GPCRs (Tang et al., 2012; Fricker and Devi, 2018). We examined whole-exome sequences (WES) from 51,289 individuals, predicted likely pathogenic variants, and then binned "likely pathogenic" plus "pathogenic" variants together. Subsequently, sequence kernel association testing (SKAT) was conducted to determine the genes that were significantly associated with the International Classification of Disease Diagnostic (ICD) codes found in the electronic health records (EHRs) of these individuals (Dershem et al., 2019). Among the top hits, the *G-protein-coupled receptor 37-like 1* (*GPR37L1*) gene was significantly associated with generalized epilepsy. Providing proof of concept for this unbiased approach, a point mutation in *GPR37L1* has previously been found in a consanguineous family with a progressive form of myoclonus epilepsy (Giddens et al., 2017). Attesting to the discovery potential of this approach, we report here that variation within the *GPR37L1* gene was also significantly associated with migraine. The encoded GPR37L1 receptor is highly expressed in astrocytes and microglia (Meyer et al., 2013; Jolly et al., 2018; Liu et al., 2018), as well as in satellite glial cells of the human trigeminal ganglia (Yang et al., 2022). Although postulated to contribute to neuroprotection, the cellular pathways have been poorly defined. In this paper, functional characterization of migraine-associated missense variants in GPR37L1 was conducted revealing agonist-induced alterations in expression, signal amplitude, and pathway bias. In addition, targeted knock-out of GPR37L1 or transient expression of certain rare variants produced alterations in cellular cholesterol homeostasis, suggesting a causal connection (Hanin et al., 2021). Finally, a knock-out (KO) mouse line lacking *Gpr37L1* was generated revealing that the loss of this receptor led to sex-specific behavioral changes implicated in migraine, but no effect on cephalic pain in an acute migraine model. Altogether, the human and mouse results focus attention on GPR37L1 as a novel, astrocytic contributor to migraine-related disorders.

Materials and Methods

Genomic analyses. To generate disease associations across the phenotype spectrum represented in the EHR, we used WES from 51,289 participants recruited through the MyCode® Community Health Initiative, which includes Geisinger patients enrolled through primary care and specialty outpatient clinics (Carey et al., 2016). Participants, who consented to broad research use of genomic data in the DiscovEHR database linked to EHR entries, were 59% female, median age of 61 years, predominantly Caucasian (98%), and non-Hispanic/Latino (95%). Sample preparation, sequencing, sequence alignment, variant identification, genotype assignment, and quality control steps were carried out as previously described (Abul-Husn et al., 2016; Carey et al., 2016; Dewey et al., 2016). Rare variants (MAF < 0.01) were sorted into loss-of-function (LOF), nonsense and frameshift, variants and missense (MISS) variants. MISS variants were further triaged by bioinformatics (RMPath score; Dershem et al., 2019) to predict benign, likely benign, likely pathogenic, and pathogenic variants, which were binned for subsequent analyses. Details of the bioinformatics triage are as previously reported (Dershem et al., 2019). Deidentified EHR data obtained from an approved data broker was sorted to identify all unique ICD9 codes with ≥200 patients with at least three independent incidences of the code. Individuals with no calls of each code were set as controls. Non-Europeans and one individual from closely related pairs up to first cousins were excluded from analyses, as non-Europeans were present in numbers too small for statistical analysis as a separate group, and closely related pairs would skew association analyses. Models were adjusted for sex, age, age^2, and first four principal components. We used the sequence SKAT with default weights (SKAT R package) to compare the burden of rare variants in cases and controls. To define the directionality of the association, all individuals with rare variants in *GPR37L1* in 51,289 WES and with EHR codes (ICD9 or ICD10) for migraine (346.*, G43.*) or epilepsy (345.*, G40.*) were identified and the RMPath scores of the variants determined, as previously described (Dershem et al., 2019). All variants were classified as "variants of unknown/uncertain significance" (VUS), that is, benign (VUSB), likely benign (VUSLB), likely pathogenic (VUSLP), or pathogenic (VUSP), according to the net scores determined by the algorithm. The primary focus of this study was migraine, but both migraine and epilepsy are diseases characterized by hyperexcitability (Rogawski, 2008); therefore, genomic analysis was designed to assess the degree of variant overlap between the two phenotypes.

Generation and culture of SK-N-MC *GPR37L1*-KO cell line. The SK-N-MC *GPR37L1*-KO cell line was generated by the CRISPR/Cas9 method (Mashiko et al., 2013). The gRNA was designed using the Optimized CRISPR Design online tool (http://crispr.mit.edu). One highly scored gRNA was found in *GPR37L1* exon 1, 5′-GCCCTAACCCCGGCAAGGAT GGG-3′. This gRNA was cloned into pSpCas9(BB)-2A-Puro (PX459) V2.0, (Addgene, #62988). The positive clone was amplified to get the plasmid after sequence analysis. The SK-N-MC cell line (ATCC, #HTB-10™) was cultured in Eagle's minimal essential medium (EMEM) medium (ATCC) with 10% fetal bovine serum (FBS) (Invitrogen). On the day of electroporation, cells were detached by 5 min treatment with StemPro Accutase (Invitrogen) and isolated by centrifugation. 5×10^6 cells were suspended in 100 µl of electroporation buffer with 20 µg plasmid, electroporated (Neon™ electroporation system, manufacturer's suggested conditions), and seeded onto three cell culture dishes (10 cm, Corning). After 24 h, puromycin (Sigma-Aldrich, 1 µg/ml) selection was initiated for 48 h. Puromycin-resistant colonies were picked mechanically using sterile 20 µl tips, and each colony was maintained in a separate well of a 48-well plate. *GPR37L1* KO clone(s) were identified by PCR and sequence analysis (forward primer, 5′-GCCCTAACCCCGGCAAGGAT-3′; reverse prime, 5′-AGTAGCTGTGCCACACGATGCACATGAC-3′). Thirteen KO clones were identified by sequence analysis. The KO clones were screened for off-target effects by Sanger sequencing for suspected genic sites that were identified by the Optimized CRISPR

Design online tool. In silico prediction determined the resemblance of genomic regions to the gRNA with up to three nucleotide mismatch tolerance; in total, three coding sites were analyzed. No alternate target modifications were observed in any of the GPR37L1-null clones compared with the sequence of the original SK-N-MC clone. Clone #40 was identified without off-target effects and was chosen for use in experimental studies (*GPR37L1*-KO SK cells). This clone has a 94-base pair deletion starting 3′ of the CRISPR/Cas9 cleavage site. The deletion caused a DNA coding sequence shift, resulting in a premature stop codon (TGA) in the sequence.

Isolation and culture of primary mouse astrocytes. Primary mouse astrocytes were cultured from postnatal Day 1–2 C57BL6 pups. Mice were quickly decapitated, and brains were removed and submerged in an ice-cold dissection medium containing 1 mM sodium pyruvate and 0.1% glucose in HEPES-buffered saline, pH = 7.4. The meninges were removed, and cortices were isolated and finely minced. A single-cell suspension was obtained by enzymatic digestion with 0.25% trypsin at 37°C for 20 min followed by trituration. Cells were seeded in a T75 flask in Dulbecco's minimal essential medium culture medium supplemented with 10% FBS and 1% penicillin–streptomycin antibiotics (Invitrogen). The medium was changed twice weekly. When cells became confluent, microglia and oligodendrocytes were removed by shaking at 260 rpm for 3 h at 37°C in an orbital shaker. Prior to biochemical assays, astrocytes were subcultured into different plates as indicated.

Generation of wild-type (WT) and GPR37L1 *variants.* The human *GPR37L1* cDNA clone (OriGene) was subcloned into pcDNA3.1+ (Invitrogen) and used as the template to insert the Glu-Glu epitope sequence (-EYMPME-) and the GPR37L1 variants used in the experiments by in vitro mutagenesis using Q5 Site-Directed Mutagenesis Kit (BioLabs). cDNA clones were confirmed by Sanger DNA sequencing (GENEWIZ). Primer sequences are available upon request.

Western blotting. WT GPR37L1 and variants (without or with the Glu-Glu tag) were transfected into *GPR37L1*-KO SK cells (SK-N-MC Transfection Kit, Altogen Biosystems). Cells were lysed after 48 h and adjusted for equivalent amounts of protein using the BCA protein assay (Thermo Scientific), and then 200 µg of lysate was incubated with an anti-Glu-Glu tag antibody (Thermo Scientific) overnight at 4°C. The next day, the immunoprecipitated complexes were pulled down by protein G beads and eluted with 5× SDS sample buffer. Eluted samples were run on 10% TGX gels (Bio-Rad), transferred to PVDF membrane (Bio-Rad), blocked with 5% milk in TBS-T, and exposed overnight at 4°C to an anti-GPR37L1 polyclonal antibody (Abcam #151518). Blots were exposed to a secondary HRP-conjugated antibody (GE HealthCare), developed with SuperSignal West Pico Chemiluminescent Substrate (Thermo Scientific), and imaged on an Odyssey Fe imager (LI-COR) and processed with Image Studio. When untagged or natively expressed receptors were studied by Western blot, membrane preparations were prepared according to the Abcam Membrane Preparation Protocol, using 500 µl of cell fractionation buffer per 10 cm dish of confluent cells, scraped into glass tubes on ice (15 min). The cell suspension was passed 10× through a 25 gauge needle and incubated on ice (20 min), and then particulates were pelleted in two rounds of centrifugation (3,000 rpm, 5 min, 4°C), combining the resulting supernatants. Membranes were then pelleted from the combined supernatants by ultracentrifugation (85,000 rpm, 40 min, 4°C), and the pellet was resuspended in the buffer. Membranes were combined with a 5× SDS sample buffer and Western blots performed as described above.

Enzyme-linked immunosorbent assay (ELISA). WT Glu-Glu-tagged GPR37L1 and Glu-Glu-tagged variants were transfected into *GPR37L1*-KO SK cells as described above. After 24 h, equivalent numbers of cells were replated to poly-L-lysine-coated 96-well plates (Corning) and further cultured for 24 h. In a subset of experiments, cells were treated for various times with 40 µM TX14(A) (Tocris). Cells were fixed with either MeOH or 4% paraformaldehyde for 15 min on ice; all further steps were carried out at room temperature. Cells were rinsed with TBS-T, blocked in 1% milk/TBS-T (1 h), then incubated with an anti-Glu-Glu tag antibody (1 h), washed, and then incubated with HRP-conjugated antibodies (1 h). Samples were developed with TMB liquid substrate supersensitive solution (Sigma-Aldrich) for 30 min and stopped with 1 M sulfuric acid. Absorbances were read at 450 nm on CLARIOstar (BMG LABTECH). Nontransfected cells were used to determine background, and blanks and background were subtracted from all samples. Three to four replicates for each condition were run in each experiment, which was repeated with at least three independent transfections.

cAMP assay. WT and variants were transfected into *GPR37L1* KO SK cells. After 48 h, cells were treated with 10 µM forskolin (FSK; Sigma-Aldrich) in DMSO ± various concentrations (0–40 µM) of TX14(A) (Tocris) in water (1 mM stock, as per manufacturer's instructions), and then cAMP levels were determined with the nonacetylated version of the direct cAMP ELISA kit (ENZO) following manufacturer's guidelines. Controls received DMSO only. Absorbance signals at 405 nm were read on a plate reader (CLARIOstar, BMG LABTECH). Optical densities were fitted to 4PL curve in Excel (Microsoft) and data analyzed with GraphPad Prism (V.8.4.3). Raw data from three independent experiments run in triplicate were combined, averaged, and analyzed.

ERK1/2 phosphorylation (ERK1/2∼P) assay. GPR37-L1-KO SK cells was cultured in an EMEM medium (ATCC) with 10% FBS (Invitrogen). On the day of electroporation, cells were detached by 5 min treatment with StemPro Accutase (Invitrogen) and isolated by centrifugation. 5×10^6 cells were suspended in 100 µl of buffer with 20 µg pcDNA3.1-*GPR37L1* plasmid, electroporated (Neon™ electroporation system, manufacturer's suggested conditions), and seeded on 60 mm cell culture dishes (Corning). After 24 h, the cells were detached by 5 min treatment with StemPro Accutase and collected by centrifugation. 30,000 cells were seeded on each well in a 96-well plate. The cells were incubated for another 24 h and then starved in 50 µl EMEM serum-free medium (antibiotic-free) in the presence or absence of a protein kinase inhibitor (PKI) (6–22amide, 50 nM, Gibco-BRL) for 3 h. The culture medium was removed, and cells were rinsed three times with warmed PBS. Cells were treated with various concentrations (0–80 µM) of TX14(A) (Tocris) for 15 min in 50 µl of EMEM in the presence or absence of a PKI at 37°C.

For the ERK1/2∼P assay, phospho- and total ERK1/2 were determined using the two-plate adherent cell protocol (Phosph-ERK1/2 kit, Cisbio), following manufacturer's instructions. Fluorescent emission signals were read at two wavelengths (665 and 620 nm) on a plate reader (CLARIOstar, BMG, LABTECH), the gain of filter setting for 665 nm is at 2,000 and for 620 nm is at 1,700, and HTRF ratios were determined, and the resulting data were analyzed with GraphPad Prism (V.8.4.3). Raw data from three independent experiments run in triplicate were combined, averaged, and analyzed.

Total cellular cholesterol assay. WT SK-N-MC cells, GPR37L1-KO cells, and GPR37L1-KO cells transiently, transfected with WT or variant GPR37L1 cDNAs, were split into 96-well plates and cultured overnight. The total cell cholesterol was measured by cleaving cholesterol esters with esterase and then complexing for 30 min in the dark at 37°C with a 50µl Amplex Red reagent/HRP/cholesterol oxidase working solution (Invitrogen). Fluorescence was measured on a plate reader (CLARIOstar, BMG LABTECH). Values were fitted to an in-plate cholesterol standard curve. Each condition was run in quadruplicate in three independent experiments, and raw data were averaged over all experiments.

Generation and validation of *Gpr37l1* knock-out mouse line. To simulate the impact of rare nonsense variants found in the large patient cohort, a KO mouse line lacking *Gpr37l1* was generated using the CRISPR/Cas9 method (Mashiko et al., 2013). The online tool (http://crispr.mit.edu) was used to identify a highly scored sgRNA within exon 1 (5′-GGTACAGCACTATGTACCCGAGG-3′), which was subsequently cloned into the pSpCas9(BB)-2A-Puro (PX459) V2.0 vector (Addgene, #62988). After confirmation of positive clones by Sanger sequencing (GENEWIZ), the plasmid was injected into the pronuclei of one-cell-stage C57BL/6J embryos according to standard protocols, and injected embryos were transferred to pseudopregnant mice (Transgenic and Gene Targeting Core, Georgia State University). From the 11 progeny, five mutant mouse pups were confirmed to have a single nucleotide deletion (C) at 3′ of the CRISPR/Cas9 cleavage site that introduced a premature stop codon (TGA), as described below. The

Gpr37l1$^{+/-}$ male mice were mated with C57BL/6J female mice (Jackson Laboratory) to produce mice carrying the deleted *Gpr37l1* allele (Gpr37L1), which were then intercrossed to produce the WT, heterozygous, and homozygous KO mice on a congenic background. To assess the potential off-target effects of the CRISPR/Cas9 technology, the KO mice were analyzed by direct Sanger sequencing for changes at suspected sites identified by the Optimized CRISPR Design online tool. In silico prediction determined the resemblance of genomic regions to the gRNA with up to three nucleotide mismatch tolerance; in total, three coding sites were analyzed, and no alternate target modifications were observed in *Gpr37l1* null mice.

For validation, genotyping was performed on genomic DNA obtained from tail clips, and PCR was performed using Taq DNA polymerase (New England Biolabs). Primers (forward primer 5′-ATCCATGCCAGACGCC TGAC) and reverse primer (5′-ATCCCCGAGTAGCCTTTGCT) were used to amplify a 722 bp fragment flanking the edited *Gpr37l1* sequence (Extended Data Figure 7-1). The amplified DNA fragment was digested with Ava1 (underlined) and subjected to agarose gel electrophoresis The PCR product from WT mice was digested into two fragments (322 and 400 bp) with Ava1, whereas the PCR products from the mutant mice could not be digested with Ava1. Subsequently, the loss of the transcript and protein was confirmed by qPCR and immunoblot analysis on mouse brains from WT, heterozygote (het), and KO (hom) mice, using an anti-GPR37L1 polyclonal antibody (GeneTex, #100005).

Animal use. All animal experiments were performed in accordance with the National Institutes of Health Guidelines for the Care and Use of Laboratory Animals and were approved by the Institutional Animal Care and Use Committee of Florida Atlantic University. For behavioral studies, animals were bred on congenic C57BL/6J line, with *Gpr37l1*-KO mice designated as *Gpr37l1*$^{-/-}$ and WT littermates designated as *Gpr37l1*$^{+/+}$. All mice were group housed (3–4/cage) and used for experiments after they reached 9 weeks of age. Animals were kept on a 12 h light/dark cycle with lights off at 7:00 P.M. in a quiet temperature-controlled room (24–25°C).

Drugs. CGRP (AnaSpec) was dissolved in PBS, used at the dose of 0.1 mg/kg (Mason et al., 2017; Rea et al., 2018), and intraperitoneally (i.p.) administered in a 5 ml/kg volume injection.

Periorbital mechanical allodynia. Behavioral assessment was conducted by an operator blinded to treatment conditions as we have recently described (Targowska-Duda et al., 2020; Sturaro et al., 2023). In brief, following an acclimation period in which mice were gently handled, habituated to i.p. injection, and held as during the test, two baseline pain measurements were conducted. To reduce variability, only the second baseline was used for data analysis. Female and male mice were tested on separate days by the same operator. von Frey filaments of different forces (0.02, 0.04, 0.07, 0.16, 0.4, 1.0, and 1.4 g) were applied to the periorbital area perpendicular to the skin, with sufficient force to cause slight buckling, and held for ∼2 s to elicit a positive response. Mice were poked five times with the same filament in a uniform manner throughout the periorbital region before changing the filament. The stimulation was initiated with the 0.16 g filament. A response occurred when the mouse stroked the face with its forelimb, withdrew its head from the stimulus, or shook its head. Sensitivity was determined according to the up-down method. The 50% mechanical withdrawal threshold (expressed in *g*) was then calculated.

Anxiety-like behavior. Anxiety-like behavior was assessed using the elevated plus maze (EPM) test as we described (Targowska-Duda et al., 2020; Sturaro et al., 2023). The EPM apparatus was a black, "plus"-shaped platform equipped with two open arms and two closed arms of the same dimensions (35.6 × 7.6 cm). The platform was at a raised height of 50 cm above the ground and placed under room lighting of 500 lux. The EPM test started when each mouse was placed on the central platform of the EPM apparatus faced to a closed arm and left free to explore the maze for 5 min. Each mouse performance was recorded by a micro camera set in the testing room and examined at a later time by an operator blinded to the treatment schedule. The operator recorded the time spent in the open arms of the maze as well as the entries into the open as measures of anxiety-like activity and the number of closed arm entries as an indicator of the mouse locomotor behavior.

Statistical analyses. TIBCO Statistica (Version 13.5.0.17) was used for data analysis. Assessment of periorbital allodynia was analyzed as area under the curve (AUC) for the various treatment combinations followed by two-way ANOVA. Unpaired *t* test was used for analysis of anxiety-like behavior in the EPM. Significance was set at $p < 0.05$.

Results

Disease associations of rare variants in *GPR37L1*

A computational approach was used to assess the clinical significance of *GPR37L1* genetic variants in 51,289 (51 K) WES. Rare [i.e., mean allele frequency (MAF) < 0.001] *GPR37L1* variants were present in the heterozygous state and classified as LOF (nonsense or frameshift) and MISS variants (Dershem et al., 2019). Although there were too few LOF variants for computational analysis, missense variants were categorized according to their predicted pathogenicity using a bioinformatics algorithm (i.e., RMPath) (Dershem et al., 2019), and 27 "likely pathogenic" or "pathogenic" variants were binned for further analysis. Subsequently, SKAT was performed by running the binned variants against all ICD9 codes with ≥200 individuals with three or more independent encounters of the code in their EHRs to ensure accuracy of disease diagnoses. As previously reported (Dershem et al., 2019) and shown here (Table 1), this unbiased approach revealed that the top disease association for *GPR37L1* variants was generalized convulsive epilepsy (ICD9 code 345.1; $Q = 6.29 \times 10^{-17}$), consistent with a published study linking *GPR37L1* with epilepsy in a consanguineous family (Giddens et al., 2017). Although the clinical phenotype of carriers was not reported, family members homozygous for the *GPR37L1* variant (p.Lys349Asn) developed a novel, progressive myoclonus epilepsy and early death by 20 years of age (Dershem et al., 2019). Also, pointing to the pleiotropic potential of this approach, epileptic seizures are commonly associated with traumatic mouth injuries (Gawlak et al., 2017), and *GPR37L1* variants were strongly linked to traumatic fracture of the tooth (ICD9 code 873,63; $Q = 3.07 \times 10^{-12}$). Likewise, *GPR37L1* variants were associated with migraine (ICD9 code 346.1 migraine; $Q = 1.13 \times 10^{-8}$), and epilepsy and migraine are known to share many clinical features and pathological mechanisms (Rogawski, 2012; Zarcone and Corbetta, 2017; Shu et al., 2020). Finally, attesting to the discovery promise of this approach, significant associations with malignant neoplasm of the kidney (ICD9 code 189) and unspecified disorder of kidney and ureter (ICD9 code 593.9) were also identified, underscoring the potential importance of GPR37L1 in vascular and renal function that has been suggested by mouse and human studies (Min et al., 2010; Coleman et al., 2018; Zheng et al., 2019; Mouat et al., 2021a,b).

Rare genomic variants in *GPR37L1* in individuals with migraine and/or epilepsy

The current study has focused on addressing the impact of genetic variation within the coding sequence of *GPR37L1* on the incidence of migraine. Since migraine and epilepsy are both diseases of hyperexcitability and associated with *GPR37L1* rare variants, we performed clinical lookups of consented patients carrying *GPR37L1* variants with the relevant diagnoses in 51,289 WES, with the goal of assessing variant overlap and/or pleiotropy. First, we assessed the three individuals heterozygous for rare nonsense (LOF) variants and found that none had three validated calls of migraine or epilepsy in their EHRs. Two were males (age range

Table 1. SKAT analysis of rare variants of *GPR37L1*

ICD9 code	Description	Variant class	*p*-value	*Q*-value	#Cases	#Controls
345.1	Generalized convulsive epilepsy, w/o mention of intractable epilepsy	MISS	1.92×10^{-19}	6.29×10^{-17}	265	50,849
873.63	Open wound of tooth (broken), uncomplicated (fractured) (trauma)	MISS	1.87×10^{-14}	3.07×10^{-12}	352	50,243
189	Malignant neoplasm of the kidney, except the pelvis	MISS	2.68×10^{-10}	2.93×10^{-08}	355	50,818
225.2	Benign neoplasm of cerebral meninges	MISS	2.11×10^{-08}	1.52×10^{-06}	205	50,970
346.1	Migraine w/o aura, w/o mention of intractable migraine, w/o mention of status migrainosus	MISS	1.13×10^{-08}	9.73×10^{-07}	1,287	48,698
593.9	Unspecified disorder of the kidney and ureter	MISS	2.63×10^{-05}	0.00075	694	48,783

Missense (MISS) variants identified in 51,289 WES of the DiscovEHR cohort were binned and subjected to SKAT analysis against the set of ICD9 codes in the EHR with at least 200 individuals with three or more independent instances of the code, regardless of genotype. Controls were specified as individuals without any instance of the code. Significance was defined as $Q < \times 10^{-5}$ with a stringent multiple-testing threshold of $p = 6.2 \times 10^{-7}$. The variants included in the analysis were as follows: c.176A > G, p.Tyr59Cys; c.356C > T, p.Pro119Leu; c.362A > G, p.Tyr121Cys; c.365C > G, p.Pro122Arg; c.379T > G, p.Ser127Ala; c.388G > A, p.Ala130Thr; c.444C > A, p.Asn148Lys; c.449C > T, p.Ser150Leu; c.476A > G, p.Tyr159Cys; c.536T > C, p.Val179Ala; c.550C > T, p.Leu184Phe; c.560T > A, p.Val187Asp; c.571G > A, p.Glu191Lys; c.588G > T, p.Arg196Ser; c.598G > A, p.Asp200Asn; c668C > T, p.Ala223Val; c.680A > G, p.Asp227Gly; c.727G > A, p.Glu243Lys; c.730C > T, p.Arg244Trp; c.823G > A, p.Glu275Lys; c.886G > A, p.Glu296Lys; c.925C > G, p.Arg309Gly; c.1081G > A, p.Val361Met; c.1141G > A, p.Val381Met; c.1171C > T, p.Arg391Cys; c.1178C > T, p.Thr393Ile; and c.1265C > T, p.Pro422Leu.

62–86) and one was a female (age 77). Next, we captured all MISS variants and used the RMPath algorithm to predict their pathogenicity scores (Fig. 1*A*). Finally, we identified the smaller set of MISS variants found in individuals with at least three encounters for migraine (ICD9 code 346.*) or epilepsy (ICD9 code 345.*). Consistent with the relative prevalence of these disorders in the adult population (Burch et al., 2015), we found a larger number of MISS variants in individuals affected with migraine than epilepsy. Moreover, a smaller number of variants were identified in individuals with both diagnoses with significant overlap of variants but not in the same individuals, suggesting a common genetic basis for these conditions (Fig. 1*A*, overlap).

Since both migraine and epilepsy are complex disorders with genetic and environmental contributors (Ragowski, 2012; Huang et al., 2017; Zarcone and Corbetta, 2017; Shu et al., 2020), the penetrance of one or the other condition in individuals carrying *GPR37L1* variants is difficult to estimate. From the EHRs, we extracted both sex and age at the first encounter for migraine and epilepsy. As shown in Table 2, carriers with a migraine diagnosis showed a significant bias toward females (~79%), while those with an epilepsy diagnosis exhibited comparable incidence among males and females (61%). The DiscovEHR 51,289 WES dataset is slightly biased toward females, that is, 59% female (Dewey et al., 2016). Thus, the relative number of variants and the differential sex bias of the two phenotypes defines sex is an additional contributor. Further, the overall frequency of migraine in individuals heterozygous for *GPR37L1* rare MISS variants was 15.5% (males/females combined), which is significantly higher than the frequency of migraine in the general Geisinger population, 10.2% (males/females combined), supporting a contribution of *GPR37L1* variant burden to migraine incidence.

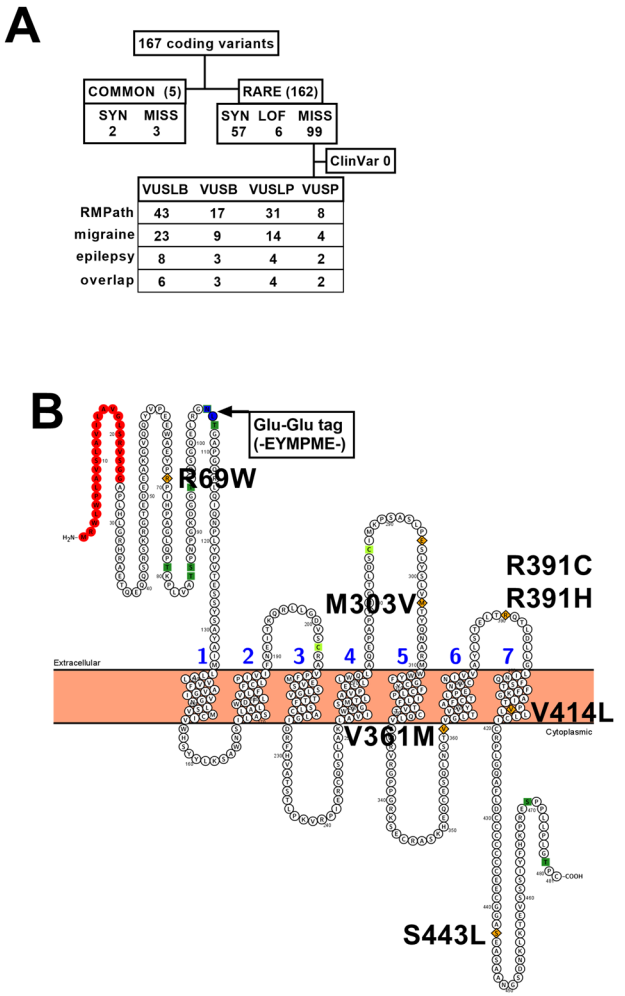

Figure 1. Pathogenicity scores of rare *GPR37L1* variants. ***A***, Flowchart of *GPR37L1* rare variants in 51,289 WES, triaged by MAF, variant type (SYN, synonymous; LOF, loss-of-function nonsense or frameshift; MISS, missense). Bioinformatics triage was done by calculating RMPath scores (Dershem et al., 2019) of all rare variants and then identifying the subset of those found in migraine (346.*) and epilepsy (345.*) patients; range of scores was from −2 to 22; maximum possible score, 24. Scores were divided into seven bins of equal width, B, benign; LB, likely benign; LP, likely pathogenic; and P, pathogenic. Overlap indicates rare variants found in both migraine and epilepsy patients (not necessarily in the same patient). ***B***, Snake plot of GPR37L1 generated with Protter software (Omasits et al., 2014) with locations of rare missense variants chosen for functional studies (p.Arg69Trp, p.Met303Val, p.Val361Met, p.Arg391His, p.Arg391Cys, p.Val414Leu, p.Ser443Leu). The location of the internal Glu-Glu tag is also indicated. Red, signal peptide residues; orange, variants studied; light green, cysteines participating in extracellular disulfide bond.

SK-N-MC cells as a viable model system to study GPR37L1 expression and function

GPR37L1 is highly expressed in astrocytes (Meyer et al., 2013) and satellite glial cells of sensory ganglia (Yang et al., 2022) and, to a lesser extent, in neurons, microglia, and oligodendrocyte precursors (Jolly et al., 2018; Liu et al., 2018). Accordingly, we identified neuroblastoma-derived SK-N-MC cells, which endogenously express this receptor, as a viable cell model to assess the impact of genetic variation on GPR37L1 expression and function. SK-N-MC cells (hereafter abbreviated SK cells) are easily transfected and used broadly for studies of cellular signaling. To provide a null background, the CRISPR/Cas9 method was used to engineer SK cells lacking GPR37L1 (KO), as confirmed by PCR screening (Fig. 2*A*) and immunoblotting analyses (Fig. 2*B*). To assess GPR37L1 signaling in SK cells, we tested

Table 2. Demographics of individuals in 51,289 WES dataset with *GPR37L1* variants

ICD9 code	Description	#Variants	#PTs	%Female	Age @ first code
345*	Epilepsy	17	28	61%	0–76
346*	Migraine	50	114	79%	13–79

All individuals with rare *GPR37L1* MISS variants with specific ICD9 codes were identified and their sex and age of onset (first incidence of ICD9 code in the EHR) of the disorder. Only parental ICD9 codes are presented. #PTS, number of patients.

fragments of the multidomain-secreted protein prosaposin (PSAP), which has been identified as the endogenous ligand of GPR37L1 in some studies (Meyer et al., 2013; Jolly et al., 2018), but contradicted in others (Coleman et al., 2016; Ngo et al., 2021). The PSAP protein is composed of four structurally similar modules, termed saposins A–D, and saposin C (SapC) is implicated in activation of GPR37L1. Because GPR37L1 is $G_{i/o}$ coupled (Liu et al., 2018), we determined the efficacies of SapC domain, or a synthetic peptide fragment derived thereof, TX14(A), on inhibition of FSK-stimulated cAMP production. GPR37L1-KO SK cells transfected with WT GPR37L1 were stimulated with FSK (10 μM) in the absence or presence of varying concentrations of either SapC or TX14(A). As shown in Figure 2*C*, both the endogenous and synthetic agonists inhibited FSK-activated cAMP generation with similar IC_{50}s (12.9 and 7.1 μM, respectively) although SapC produced a more robust inhibition of cAMP generation. The TX14(A)-mediated inhibition of cAMP production is present in WT SK cells but notably absent in *GPR37L1*-KO SK cells (Fig. 2*D*). Likewise, TX14(A) showed a greater than 50% reduction in FSK-mediated cAMP production in primary astrocytes (Fig. 2*E*). Taken together, these results demonstrate that WT SK cells express GPR37L1 as the sole target of TX14(A), and thus *GPR37L1*-KO SK cells provide the appropriate cellular context for comparison of signaling by WT and variant GPR37L1.

Functional analysis of GPR37L1 variants associated with migraine

For functional analyses, we chose GPR37L1 variants across the range of predicted pathogenicity located at sites conserved in the human and mouse to broaden the long-term impact of these studies, that is, VUSB, p.Met303Val and p.Val414Leu, VUSLB, p.Arg69Trp, p.Ser443Leu and p.Arg391His, and VUSLP, p.Val361Met, and p.Arg391Cys. Fortuitously, two variants with different predicted pathogenicities were identified at Position 391, that is, p.Arg391His (likely benign, RMPath score 8) in a single individual with no instances of relevant phenotypes, and p.Arg391Cys (likely pathogenic, RMPath score 15), found in two individuals, one with migraine. Table 3 summarizes the variants chosen and patient demographics, if any. Since bioinformatics predictions cannot account for variant-mediated changes of secondary or tertiary structure or at binding sites, the variant locations are marked in relation to the topology of the receptor (Fig. 1*B*), that is, in the N-terminal domain (p.Arg69Trp), ECL2 (p.Met303Val), at the junction of the ICL3 and helix 6 (p.Val361Met), ECL3 (p.Arg391His, p.Arg391Cys), toward the cytoplasmic end of helix 7 (p.Val414Leu), and in the C-terminal segment (p.Ser443Leu).

Functional analyses of these variants were performed in KO SK cells expressing either WT or variant receptors, and the relative abilities of TX14(A) to attenuate FSK-stimulated cAMP production (Meyer et al., 2013) were measured (Fig. 3, Table 4). We noted four distinct changes in signaling. Two receptor variants [p.Met303Val (VUSB), p.Arg391His (VUSLB)] had signaling properties indistinguishable from the WT receptor in the presence or absence of TX14(A) (Fig. 3*Aa*). Two other receptor variants [p.Val414Leu (VUSB), p.Ser443Leu (VUSLB)] were more effective at reducing cAMP than WT receptor in the presence of an agonist (Fig. 3*Ab*). Likewise, two receptor variants [p.Val361Met (VUSLP), p.Arg391Cys (VUSLP)] were more effective at reducing cAMP than the WT receptor in the presence of TX14(A), but also showed significantly reduced cAMP in the absence of the agonist, indicative of basal constitutive activity (Fig. 3*Ac*). The final receptor variant [p.Arg69Trp (VUSLB)] was less effective at inhibiting cAMP than the WT receptor in the presence of TX14(A) (Fig. 3*Ad*). Figure 3*B* summarizes the diverse range of basal and TX14(A)-inhibited cAMP levels as well as apparent alterations relative to WT for each variant. Overall, these results show only a weak correlation between bioinformatics-based predictions of pathogenicity and experimental analysis of receptor variants, with analysis of receptor activity revealing altered signaling properties of most receptor variants.

GPR37L1 also regulates mitogen-activated protein kinase (MAPK) pathways (Meyer et al., 2013); therefore, we next tested the ability of WT and receptor variants to activate ERK1/2∼P (Fig. 4*A*). We noted three patterns of signaling alterations. Three receptor variants, two with normal cAMP inhibition (p.Met303Val, p.Arg391His) and one with increased potency for cAMP inhibition (p.Ser443Leu), had agonist-induced ERK1/2∼P comparable to the WT receptor (Fig. 4*Aa*). Three receptor variants (p.Val414Leu, p.Val361Met, p.Arg391Cys) with enhanced cAMP inhibition were found to have reduced ERK1/2∼P relative to WT in response to the agonist (Fig. 4*Ab*). The last variant (p.Arg69Trp), with lower cAMP inhibition, had an apparent increase in E_{max} (Fig. 4*Ac*) which was not well fitted over the accessible TX14(A) concentration range, although there was a significant, reproducible increase in ERK1/2∼P at 60 and 80 μM TX14(A) (Fig. 4*Ac*). Despite variable changes in E_{max}, all receptor variants had fitted EC_{50}s comparable to the WT receptor. Finally, we tested whether there was interaction between the cAMP and MAPK pathways by measuring ERK1/2∼P in cells expressing WT GPR37L1 in the absence or presence of 50 nM protein kinase A inhibitor peptide (PKI). As illustrated in Figure 4*C*, addition of PKI had no impact on ERK1/2∼P in the presence or absence of TX14(A). Taken together, these results demonstrate that a subset of GPR37L1 variants found in patients with a migraine diagnosis showed changes in agonist-induced cAMP inhibition and ERK1/2∼P that may be indicative of changes in signaling bias.

Impact of migraine-associated variants on GPR37L1 expression and localization

To determine whether the signaling differences among GPR37L1 variants could in part be due to altered expression and/or subcellular distribution, we incorporated an epitope tag that allows net expression and plasma membrane targeting to be accurately assessed. Because GPR37L1 can be cleaved by endoproteases at N-terminal sites (Coleman et al., 2016, 2020), the epitope tag was inserted at a site in the amino terminus distal to potential GPR37L1 cleavage sites to ensure accurate assessment of expression levels. The small Glu-Glu epitope tag (-EYMPME) was introduced between residues p.Asn105 and p.Leu106 at the extracellular amino terminus (indicated in Fig. 1*B*). Tagged WT GPR37L1 (=Glu-GPR37L1) allowed efficient immunoprecipitation (IP) of transfected receptors from KO SK cells. Figure 5*A* illustrates a Western blot that compares the sizes of untagged

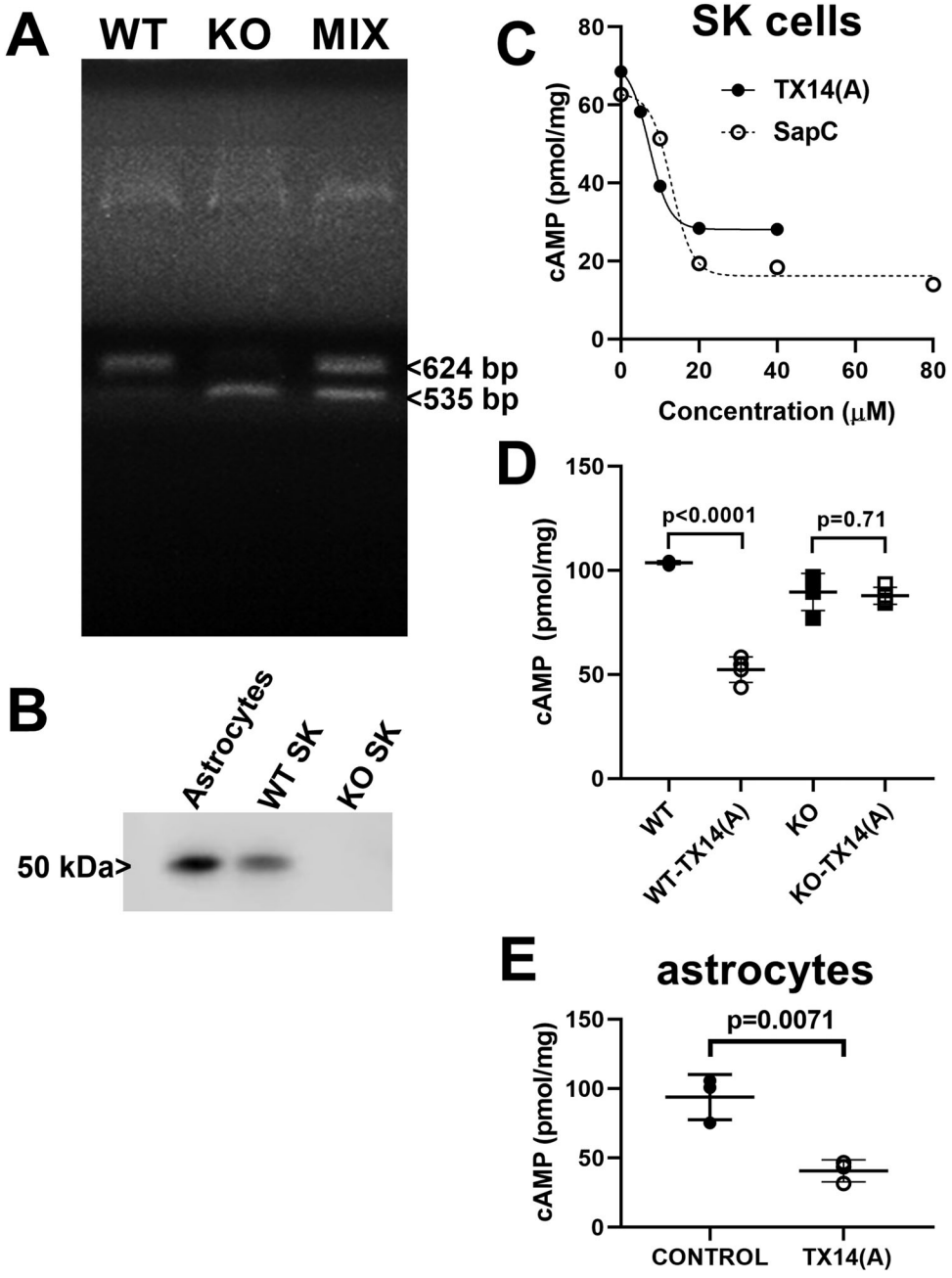

Figure 2. GPR37L1 expression and function in SK-N-MC cells. ***A***, RT-PCR demonstrating endogenous expression of GPR37L1 in SK-N-MC cells (WT) and RT-PCR validation of a CRISPR/Cas9-generated *GPR37L1*-KO SK cell clone (KO). Final lane shows gel run of mixture of both PCR products (MIX). ***B***, Western blot of membrane preparations from primary mouse astrocytes, WT and *GPR37L1*-KO SK cells, probed with an anti-GPR37L1 antibody (Abcam). Membranes were isolated as described in Materials and Methods; 30 μg of membranes per lane. Full blot of GPR37L1 in Extended Data Figure 2-1. ***C***, The PSAP module SapC and TX14(A) (Thr-D-Ala-Leu-Asp-Asn-Asn-Ala-Thr-Glu-Glu-Ile-Leu-Tyr) (Meyer et al., 2013) activate GPR37L1. Control SK-N-MC cells were stimulated with 10 μM FSK ± different concentrations of the peptide TX14(A) (IC_{50} 7.2 μM) or SapC (IC_{50} 12.9 μM). cAMP was analyzed as described in Materials and Methods. Curves were generated by fitting all raw data from three independent experiments. ***D***, WT and *GPR37L1*-KO cells were stimulated with 10 μM FSK ± 40 μM TX14(A), and cAMP levels were assayed as described in Materials and Methods. ***E***, Primary mouse astrocytes were stimulated with 10 μM FSK ± 40 μM TX14(A), and cAMP levels were assayed as described in Materials and Methods. Significances in ***D,E*** were determined by two-tailed *t* test assuming unequal variances, $*p < 0.05$, $**p < 0.01$, $***p < 0.001$, $****p < 0.0001$.

WT GPR37L1 (MembWT) and WT Glu-GPR37L1 (IP). The blot was probed with a polyclonal anti-GPR37L1 antibody, and both Glu-GPR37L1 and the untagged WT GPR37L1 had a dominant band consistent with the predicted mass of the full-length receptor. Glu-GPR37L1 had a slightly larger mass than the untagged version, as expected. There was no evidence for proteolytic cleavage of the receptor in this cell line (Fig. 5*B*).

Detection of Glu-tagged WT and variant receptor was performed by Western blotting (Fig. 5*C*), while surface and total expressions were quantified by ELISA (Fig. 5*D*). Although most variants were comparably expressed to WT (surface expression, Fig. 5*Da*; total expression, 5 Db), two receptor variants (p.Val361Met and p.Arg391Cys) exhibited a reduced total expression relative to WT and thus higher surface to total expression ratios (Fig. 5*Dc*). As changes in surface expression of receptors can produce significant alterations in downstream signaling, it is interesting to note that both variant receptors also showed enhanced cAMP inhibition (recall Fig. 3*Ac*). Surprisingly, we

Table 3. *GPR37L1* migraine-associated variants selected for functional studies

Variant rs ID	RMPath class	RMPath score	HO_HE	345.*	346.*
p.Arg69Trp rs1219056911	VUSLB	9	0_5	F/21 years	F/20 years F/22 years
p.Met303Val rs771579982	VUSB	15	0_4	None	F/23 years; F/23 years
p.Val361Met rs114687119	VUSLP	11	0_6	None	None
p.Arg391Cys rs772132535	VUSLP	15	0_2	None	F/37 years
p.Arg391His rs773384673	VUSLB	8	0_1	None	None
p.Val414Leu rs141962107	VUSB	4	0_6	None	F/27 years; F/15 years
p.Ser443Leu rs748607219	VUSLB	7	0_3	None	None

Indicated are the number of homozygous or heterozygous individuals (HO_HE) in 51,289 WES with the variant (rs ID indicated) and details of the individuals with the indicated calls for epilepsy (345.*) and/or migraine (346.*). Three variants had no individuals with indicated phenotypes and were included to test the range of pathogenicity scoring on function.

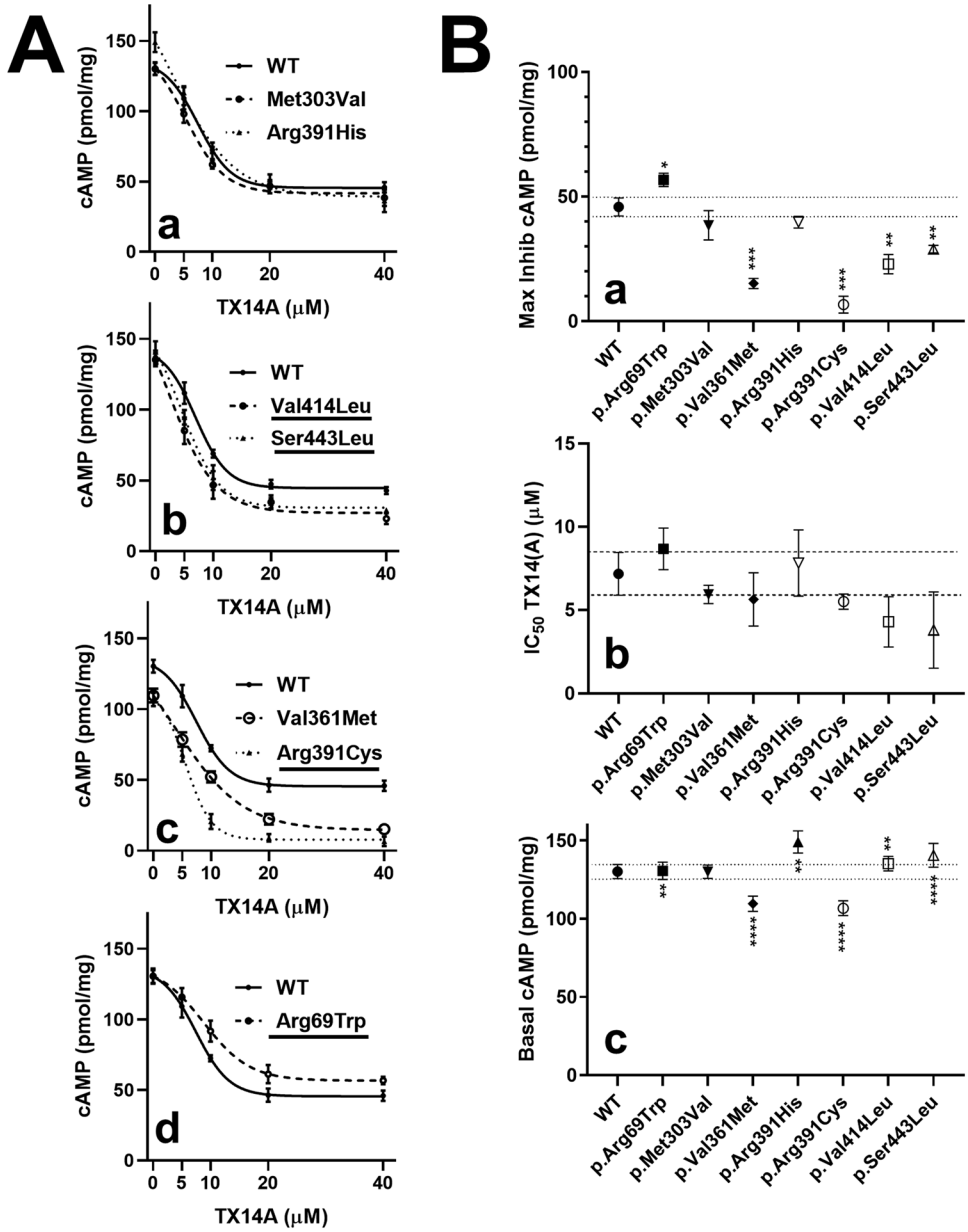

Figure 3. Migraine-associated variants in transfected *GPR37L1*-KO cells have differential ability to inhibit cAMP production. ***A***, Migraine-associated variants were assessed for their ability to attenuate FSK-stimulated cAMP production when activated by TX14(A). *GPR37L1*-KO cells were transiently transfected with WT or variants, and net cellular cAMP was determined at a range of TX14(A) concentrations in cells stimulated with 10 μM FSK, as described in Materials and Methods. Plots present averaged raw data ± SD results of three independent transfections. Variants are plotted with WT (solid line in all graphs), according to their different patterns of response. ***a***, p.Met303Val (dashed line), p.Arg391His (dotted line). ***b***, p.Val414Leu (dashed line), p.Ser443Leu (dotted line). ***c***, p.Val361Met (dashed line), p.Arg391Cys (dotted line). ***d***, p.Arg69Trp (dashed line). ***B***, Quantitation of at least three independent experiments as illustrated in ***A***. Inhibition curves were fitted and the maximal inhibition by TX14(A) (***a***), the IC_{50} for TX14(A) (***b***), and basal cAMP levels (***c***), zero TX14(A), were determined as described in Materials and Methods. Statistical differences were determined by two-tailed Student's *t* test, compared with WT responses, with $*p < 0.05$, $**p < 0.01$, $***p < 0.001$, $****p < 0.0001$.

Table 4. Summary of functional differences between WT and GPR37L1 variants

Variant	cAMP[a] mean ± SD (pmol/mg)		ERK∼P[b] HTFR units	TX14(A) on surface/total ratio[c]	Cholesterol levels[d] μM	
	FSK-	FSK TX14(A)	SPAN ± SD	% ± SD	Basal	TX14(A)
WT	130.2 ± 4.5	45.83 ± 3.6	31.65 ± 3.1	62.3 ± 0.1.3	12.6 ± 0.45	14.2 ± 0.33
p.Arg69Trp	130.7 ± 5.5	56.69 ± 2.7*	44.4 ± 11.0	59.8 ± 4.3	12.4 ± 0.35	13.6 ± 0.2*
p.Met303Val	130.1 ± 4.3	38.49 ± 5.9	No fit	62.0 ± 0.85	12.4 ± 0.14	13.6 ± 0.1*
p.Val361Met	109.6 ± 4.9**	15.7 ± 2.0****	41.1 ± 4.5*	87.0 ± 7.8****	12.8 ± 0.34	13.1 ± 0.1****
p.Arg391Cys	106.8 ± 4.7***	6.68 ± 3.4****	41.0 ± 6.5	85.2 ± 6.7***	12.3 ± 0.53	12.6 ± 0.2****
p.Arg391His	149.3 ± 7.1**	39.76 ± 2.4	30.8 ± 1.4	66.2 ± 3.2	12.6 ± 0.16	14.2 ± 0.1
p.Val414Leu	135.2 ± 4.7	22.92 ± 3.9****	29.1 ± 1.5*	58.9 ± 3.3	12.4 ± 0.21	13.8 ± 0.1
p.Ser443Leu	140.6 ± 7.6	28.92 ± 1.5***	30.8 ± 1.4*	66.8 ± 6.0	12.5 ± 0.22	14.3 ± 0.2
KO	-	-	-	-	0.82 ± 0.5****	10.1 ± 0.2****

Functional differences among variants for basal and TX14(A)-mediated signaling.
[a]FSK-mediated cAMP production in the absence and presence of 40 μM TX14(A). IC_{50}s for TX14(A)-mediated inhibition of cAMP production were not different from WT (one-way ANOVA, data not shown), but variant-specific differences from WT were observed for both cAMP levels in the absence (FSK, 10 μM) and presence of TX14(A) (FSK, 10 μM), that is, at maximum inhibition, as indicated (one-way ANOVA with multiple comparisons). *$p < 0.05$, **$p < 0.01$, ***$p < 0.001$, ****$p < 0.0001$.
[b]There were no significant differences among WT and variants in the EC_{50} for ERK phosphorylation (one-way ANOVA, data not shown). However, there were differences in the span of activation (maximum − minimum) elicited by 80 μM TX14(A), as indicated. Analysis by one-way ANOVA with multiple comparisons, *$p < 0.05$.
[c]The effect of 30 min incubation in 40 μM TX14(A) on surface/total GPR37L1 protein levels assessed by ELISA, analyzed by one-way ANOVA with multiple comparisons, ***$p < 0.001$, ****$p < 0.0001$.
[d]Cholesterol levels were measured in the absence (basal) and after treatment with 40 μM TX14(A) for 30 min, analyzed by one-way ANOVA with multiple comparisons, *$p < 0.05$, ****$p < 0.0001$.

also found that short-term treatment with TX14(A) produced an upregulation of GPR37L1 (Fig. 5*A*). To explore the nature of this effect and to assess the potential impact of receptor variants, KO SK cells expressing Glu-tagged WT or variant receptors were treated with TX14(A) (30 min, 40 μM). First, we determined that the Glu tag did not affect receptor signaling. Both WT Glu-GPR37L1 and the untagged WT GPR37L1 inhibited FSK-mediated accumulation of cAMP with comparable IC_{50}s (Fig. 5*E*). Thus, the Glu tag does not alter key features of the WT receptor and was therefore used to assess changes in expression and/or signaling by GPR37L1 variants.

Although the maximal extent varied, agonist treatment caused rapid, time-dependent increases in their expression, with receptor variants p.Val361Met and p.Arg391Cys with the weakest upregulation (Fig. 5*F*). It is of note that p.Arg391His has signaling equivalent to WT in both cAMP and ERK1/2∼P assays and shows net expression and upregulation comparable to WT, while the p.Arg391Cys variant has enhanced basal activity and decreased EC_{50} in the cAMP inhibition assay, and reduced E_{max} in the ERK1/2∼P assay, and significantly less TX14(A)-mediated upregulation. Altogether, these results demonstrate the impact of *GPR37L1* genetic variation on signaling efficacy, bias, and expression, with p.Arg391Cys and p.Val361Met showing changes across all three metrics. Results also reveal a rapid upregulation of GPR37L1 expression in response to agonist treatment that is dependent upon receptor occupancy and/or signaling output(s).

GPR37L1 and total cellular cholesterol levels

Perturbations in brain cholesterol homeostasis are linked to neurological disorders including migraine, in which hyperexcitability may play a role (Hanin et al., 2021). To assess the importance of GPR37L1 to cholesterol homeostasis, WT and KO SK cells and KO cells transiently transfected with or without GPR37L1 receptor were used (Fig. 6*A*). A comparison of total cholesterol content among these cell lines revealed that the loss of endogenous expression of GPR37L1 significantly reduced cholesterol content (Fig. 6*B*, compare WT and KO cells), while transient transfection of the WT receptor restored cholesterol abundance to a normal level. Of even more interest, acute treatment of cells expressing endogenous or exogenous GPR37L1 with the agonist TX14(A) for 30 min produced statistically significant increases in total cholesterol, which was not observed in KO cells lacking the receptor (Fig. 6*B*). These results point to a novel role for GPR37L1 in the acute regulation of cholesterol homeostasis in response to the agonist.

Since treatment with TX14(A) enhanced the differences in cellular cholesterol levels between WT and KO SK cells, we used the same approach to compare the total cellular cholesterol levels in KO cells transiently transfected with WT or variant GPR37L1. In the absence of TX14(A), cells expressing WT or receptor variants had equivalent amounts of total cell cholesterol, while there was an ∼20% lower level in the KO SK cell line (Fig. 6*Ca*). However, agonist treatment revealed differential responses between WT and receptor variants. Two receptor variants (p.Arg69Trp and p.Met303Val) showed weaker responses compared with WT, while two others (p.Val361Met and p.Arg391Cys) failed to increase total cholesterol levels in response to TX14(A) (Fig. 6*Cb*). Variant responses to TX14(A) are plotted in Figure 6*D*. Of particular note, two receptor variants (p.Arg391Cys and p.Val361Met) with altered signaling properties in both cAMP and ERK1/2 assays failed to significantly increase total cholesterol levels in response to acute treatment with TX14(A). The different variants at position p.Arg391 again showed differential responses, that is, TX14(A) elicited no cholesterol increase in cells expressing p.Arg391Cys, while cells expressing p.Arg391His had an increase in total cholesterol in TX14(A) similar to WT.

Acute regulation of total cell cholesterol by GPCRs has not been fully characterized, although a recent study has demonstrated neuropeptide Y-mediated upregulation of cholesterol in liver cells, a response that could be blocked by the MEK1/2 inhibitor U0126 (Chen et al., 2020). Here, we determined whether the MAPK pathway contributed to the TX14(A)-mediated upregulation of total cholesterol in WT SK cells. As we have shown (Fig. 4), TX14(A) increases ERK1/2 phosphorylation, and we hypothesized that blocking the upstream activator of ERK1/2 with U0126 should prevent TX14(A)-mediated increases in cellular cholesterol. Figure 6*E* illustrates that TX14(A) caused a significant increase in total cholesterol in WT SK cells. WT SK cells had higher total cholesterol levels than KO SK cells, suggesting some constitutive activity of the endogenous GPR37L1 in WT SK cells. The U0126 had no effect on unstimulated WT or KO SK cells, but when treated with TX14(A), the U0126 severely attenuated the increase in cholesterol in WT SK cells. Overall, the results demonstrate

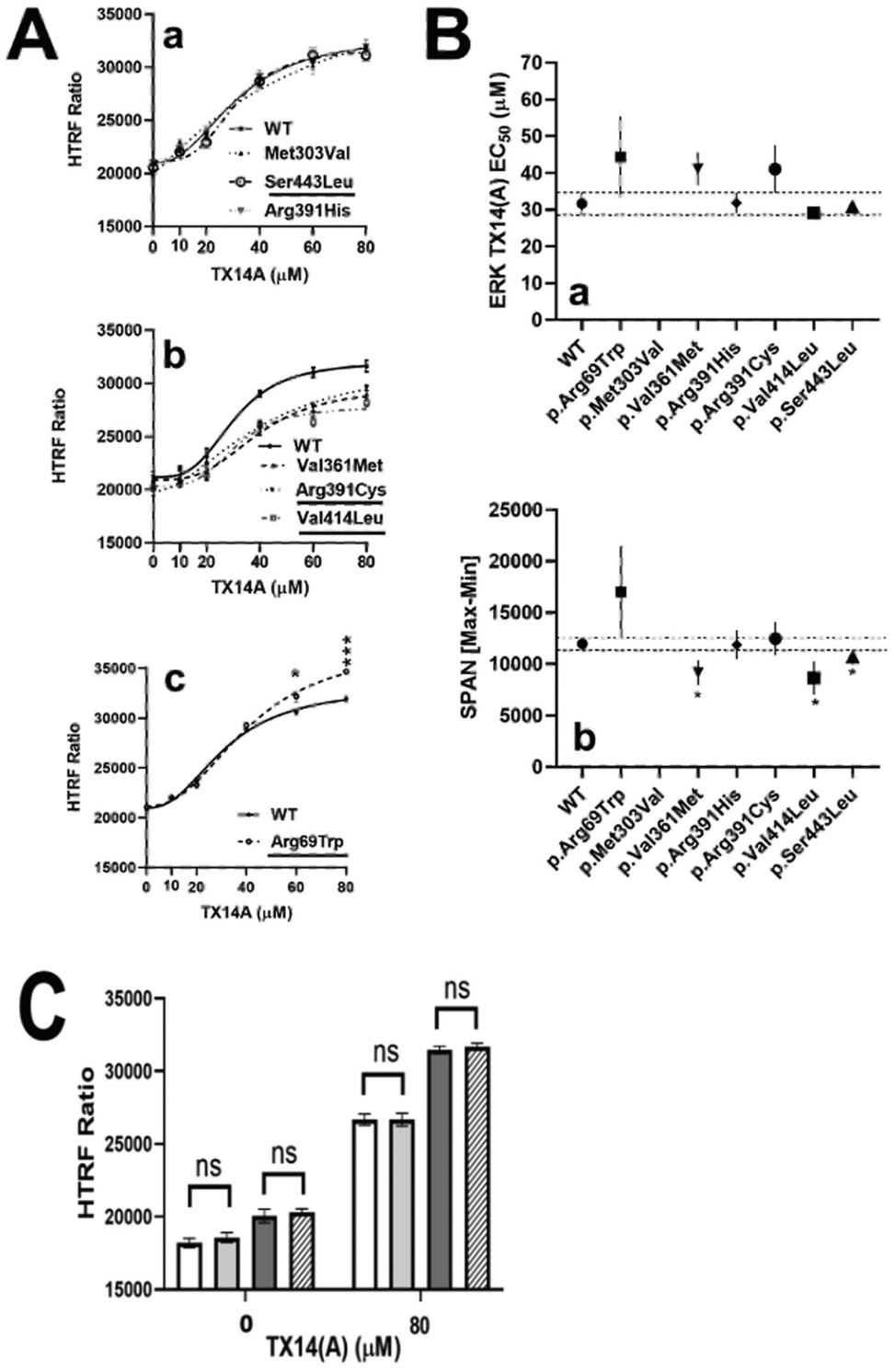

Figure 4. Migraine-associated variants in transfected *GPR37L1*-KO cells have differential ability to stimulate ERK1/2∼P. ***A***, The ability of TX14(A) to induce ERK1/2∼P in *GPR37L1*-KO cells transfected with WT or variants was determined in a plate-based assay as described in Materials and Methods. Plots illustrate averages from three independent transfections. Variants were plotted with WT (solid line) and sorted by their response differences. Variants found in patients with migraine are underlined in all plots. ***a***, p.Met303Val (dashed line), p.Arg391His (dotted line), p.Ser443Leu (dash-dotted line). ***b***, p.Val361Met (dashed line), p.Arg391Cys (dotted line), p.Val414Leu (dash-dotted line). ***c***, p.Arg69Trp (dashed line). ***B***, Stimulation curves were fitted and the EC_{50} estimates (***a***) and the span (maximum − minimum) (***b***) were determined as described in Materials and Methods. Statistical differences were determined by two-tailed Student's *t* test, compared with WT responses, $*p < 0.05$, $**p < 0.01$, $***p < 0.001$, $****p < 0.0001$. ***C***, Interaction of cAMP and MAPK pathways in GPR37L1 responses was tested by treatment of KO cells or cells transfected with WT GPR37L1, with 50 nM PKI, showing its addition had no impact on ERK1/2∼P in the presence or absence of TX14(A), as determined by one-way ANOVA analysis. ☐ KO cells, ☐ KO cell + PKI, ■ WT cells, ▨ WT cell + PKI. Three independent experiments were run in triplicate. NS, not significant.

that acute stimulation of GPR37L1 contributes significantly to total cellular cholesterol homeostasis through activation of MAPK pathways.

Role of GPR37L1 in migraine-related disorders

To simulate the impact of rare nonsense variants found in the large patient cohort, a KO mouse line lacking *Gpr37l1* was generated on

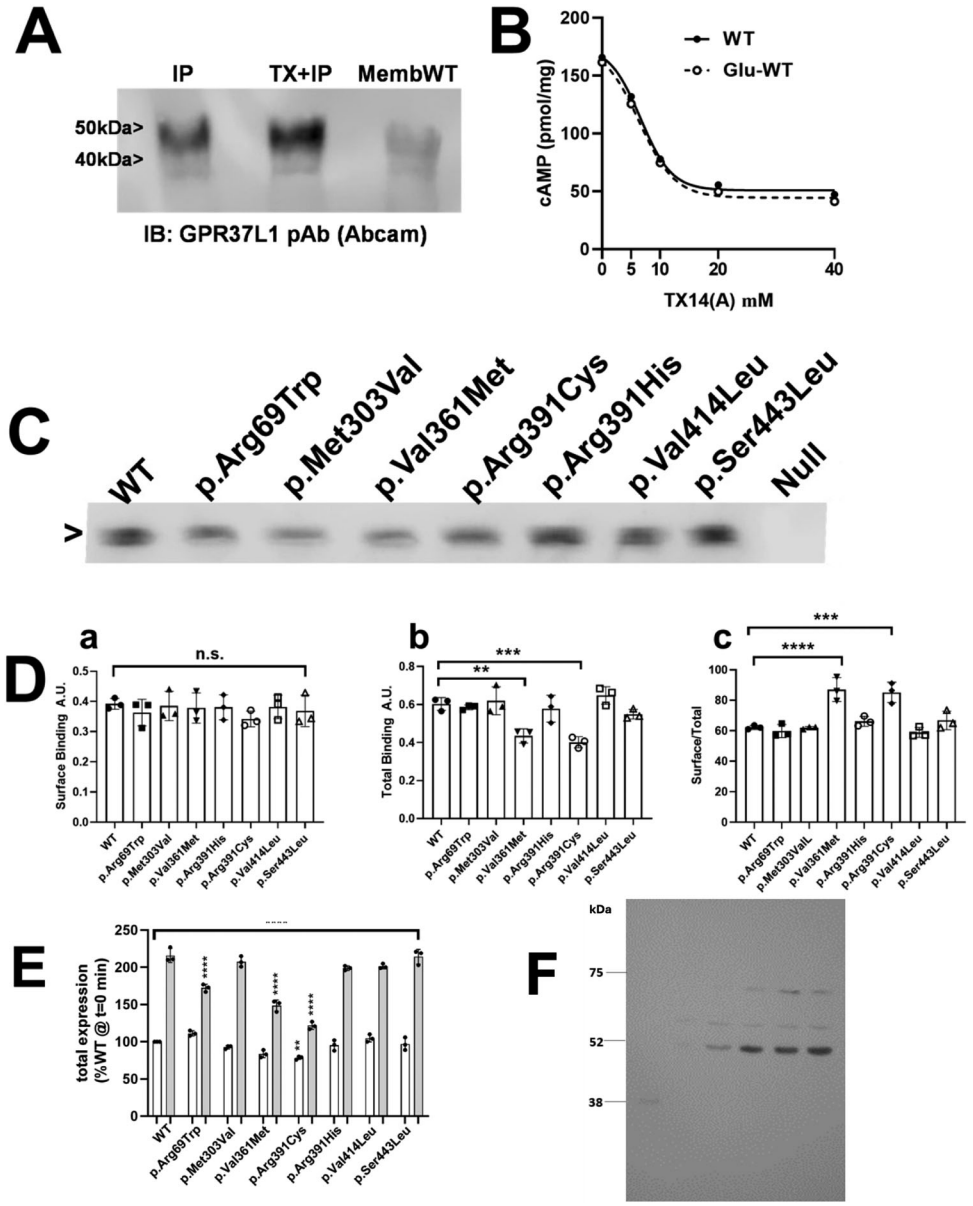

Figure 5. Variant-associated changes in GPR37L1 expression or localization. ***A***, *GPR37L1*-KO SK cells were transfected with either untagged WT or Glu-*GPR37L1*, followed by IP with an anti-Glu antibody or isolation of membranes to assess untagged GPR37L1. A second Glu-*GPR37L1*-transfected sample was treated ± 40 µM TX14(A) (30 min) prior to IP. Blot was probed with an anti-GPR37L1 polyclonal antibody (Abcam). ***B***, Western blot analysis. Whole-cell extracts (50 µg) were separated by 10% SDS-PAGE, and the membrane was blotted with a rabbit anti-GPR37L1 polyclonal antibody (GeneTex, GTX10005) diluted at 1:1,000. Subsequently, the HRP-conjugated goat anti-rabbit IgG antibody (1:10,000, Jackson ImmunoResearch Laboratories) was used to detect the primary antibody, revealing the absence of a ∼52 kDA band in GPR37L1-KO SK cells (Lane 1) versus its presence in WT SK cells (Lane 2) and in GPR37L1-KO SK cells that were transfected with pcDNA-GPR37L1 in three different experiments (Lanes 3–5). Notably, there was no evidence of smaller bands associated with N-terminal cleavage. ***C***, *GPR37L1*-KO SK cells transfected with Glu-tagged WT or variant *GPR37L1*, immunoprecipitated with anti-Glu antibodies, and analyzed by Western blot probed with an anti-GPR37L1 antibody (see Materials and Methods). ***D***, ELISA assays of Glu-tagged WT or variants assessing surface (left panel, fixed with paraformaldehyde) or total (middle panel, fixed with cold methanol) expression in the absence of TX14(A). The right panel illustrates the surface / total distribution of WT and variants. Data presents mean of all points (4 replicates×3 independent experiments) or mean ± SD (right panel). Statistical analysis by two- way ANOVA with multiple comparisons, $*p < 0.05$, $**p < 0.01$, $***p < 0.001$, $****p < 0.0001$. ***E***, Response of *GPR37L1*-KO SK cells transfected with either WT or Glu-GPR37L1 to TX14(A) inhibition of FSK-mediated cAMP production. ***F***, ELISA assays to assess total expression of GPR37L1 were used to compare basal (no TX14(A), white bars) and 30 min in 40 µM TX14(A) (gray bars) for WT and GPR37L1 variants. Three independent experiments were run in quadruplicate, and mean protein levels for each experiment were averaged and normalized to WT at zero time or after 30 min treatment with TX14(A). Data were analyzed by one-way ANOVA with multiple comparisons, and significance is indicated as $*p < 0.05$, $**p < 0.01$, $***p < 0.001$, and $****p < 0.0001$.

a congenic background to assess its role in neurological processes and permit dissection of the underlying mechanism(s) (Fig. 7). For the initial in vivo characterization, we focused on two migraine-related behaviors that share similar clinical features and suspected pathophysiology. For the acute migraine phenotype, we relied on a widely used model for migraine pathophysiology, acute CGRP injection, which produces facial pain sensitivity as measured by von Frey monofilaments (Mason et al., 2017; Rea et al., 2018; Sturaro et al., 2023). In this case, KO and WT littermates showed increased pain sensitivity following a single CGRP injection that was indistinguishable between the two genotypes in female and male mice. Two-way ANOVA, conducted to analyze possible

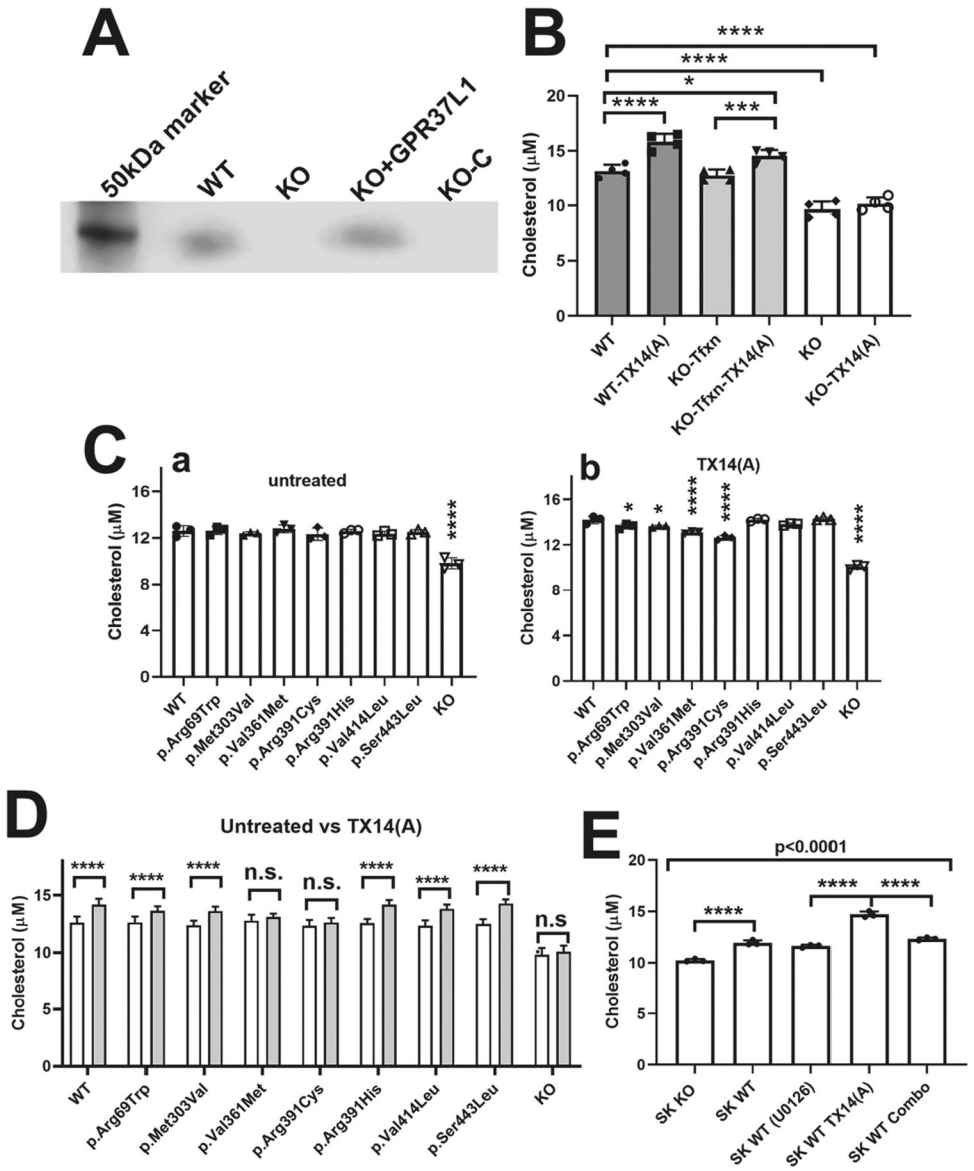

Figure 6. GPR37L1 regulation of cellular cholesterol levels. ***A***, Western blot of WT SK cells, *GPR37L1*-KO cells, KO cells transfected with WT G*PR37L1*, or KO cells exposed to a transfection reagent (KO-C), blotted with an anti-GPR37L1 antibody (Abcam). ***B***, Total cellular cholesterol levels in WT SK cells, *GPR37L1*-KO cells transfected with WT *GPR37L1*, or *GPR37L1*-KO cells, treated with vehicle or 40 μM TX14(A) for 30 min. ***C***, Total cellular cholesterol was measured in *GPR37L1*-KO cells transfected with WT or variants and treated without (***a***) or with 40 μM TX14(A) (***b***) for 30 min. Analysis of ***B*** and ***C*** was performed by two-way ANOVA with multiple comparisons, relative to WT under the same condition, $*p < 0.05$, $**p < 0.01$, $***p < 0.001$, $****p < 0.0001$. ***D***, Comparison of total cellular cholesterol changes evoked by 40 μM TX14(A) treatment for 30 min, in WT or variant-transfected *GPR37L1*-KO cells. White, untreated, black, TX14(A)-treated. Analysis by Student's *t* test, $*p < 0.05$, $**p < 0.01$, $***p < 0.001$, $****p < 0.0001$. ***E***, Impact of U0126 on total cholesterol levels was assessed by treatment with either U0126 alone or in the presence of TX14(A) (=Combo), using WT SK cells. KO SK cells were used as a control, and treatment with U0126 had no effect on cholesterol levels in the absence of GPR37L1 (data not shown). Significance was determined by one-way ANOVA with multiple comparisons, with $*p < 0.05$, $**p < 0.01$, $***p < 0.001$, $****p < 0.0001$.

differences in allodynic responses calculated as AUC in *Gpr37l1*$^{-/-}$ versus *Gpr37l1*$^{+/+}$ female mice treated with or without CGRP, led to a significant main effect of CGRP treatment [$F_{(1,46)} = 4.4$; $p = 0.04$] accompanied by the lack of a genotype effect [$F_{(1,46)} = 0.6$; $p = 0.38$] and "treatment × genotype" interaction [$F_{(1,46)} = 0.0$; $p = 0.76$; Fig. 8*A*]. In male mice, there was a significant effect of CGRP treatment [$F_{(1,45)} = 18.3$; $p = 0.0001$], which, similarly to the outcome in females, was not accompanied by a significant genotype effect [$F_{(1,45)} = 1.0$, $p = 0.315$] or interaction [$F_{(1,45)} = 0.4$; $p = 0.534$; Fig. 8*B*]. One possibility for the lack of difference in the CGRP effects between WT and KO animals is that the CGRP dose was too high. However, the use of lower CGRP dose also revealed no difference (Fig. 8*C*). Collectively, these results suggest that a single CGRP treatment evoked periorbital mechanical allodynia in male and female mice. However, the loss of *Gpr37l1* did not affect the response to acute CGRP treatment.

For the anxiety-related characterization, we used an established paradigm, the EPM, which measures time spent in the open versus enclosed arms (Targowska-Duda et al., 2020; Sturaro et al., 2023). To assess the effect of genetic disruption of the *Gpr37l1* gene on anxiety phenotype, we compared their behavior in the EPM paradigm. Unpaired *t* test revealed that female *Gpr37l1*$^{-/-}$ mice significantly spent less time than WT mice on the open arms of the EPM [$t_{(20)} = 4.9$; $p < 0.0001$; Fig. 9*A*]. In contrast, male *Gpr37l1*$^{-/-}$ mice showed similar open arm time to WT (*Gpr37l1*$^{+/+}$) mice [$t_{(14)} = 0.9$; $p = 0.359$; Fig. 9*B*]. Mutant *Gpr37l1*$^{-/-}$ female mice also entered the

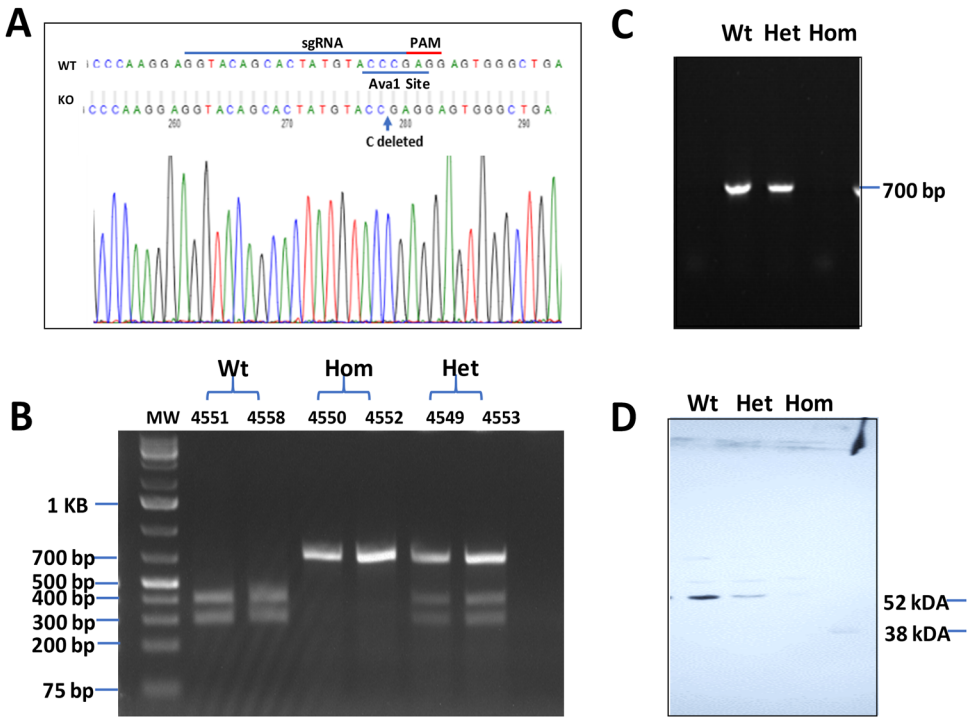

Figure 7. Generation and validation of *Gpr37l1* KO mice. ***A***, Schematic representation of sgRNA targeting sequence and PAM site in the mouse *Gpr37l1* exon 1 region. The Ava1 recognition sequence is underlined, and a single base pair "C" deletion in *Gpr37l1* KO mice is indicated in sequence. ***B***, Genotyping of WT and *Gpr37l1*-KO mice. A 722 bp PCR product was amplified with a pair of primers that flanked the gene-edited sequence of *Gpr37l1*. The PCR product from WT mice was digested into two fragments (322 and 400 bp) with Ava1. However, the PCR products from the mutant mice could not be digested with Ava1. ***C***, RT-PCR shows the relative quantity of *Gpr37l1* mRNA extracted from mouse brains in the WT, heterozygote (het), and KO (hom) mice. ***D***, Western blot analysis of protein expression in the brains of WT, het, and KO mice.

open arms of the maze less than $Gpr37l1^{+/+}$ mice [$t_{(20)} = 3.7$; $p = 0.0014$; Fig. 9*C*], whereas male $Gpr37l1^{-/-}$ mice performed similarly to WT [$t_{(14)} = 1.2$; $p = 0.238$; Fig. 9*D*]. $Gpr37l1^{-/-}$ mice of both sexes exhibited similar exploration of the maze, as shown by similar entries onto the closed arm of the EPM [females: $t_{(20)} = 0.4$, $p = 0.685$; males: $t_{(14)} = 2.0$, $p = 0.0613$; Fig. 9*E*,*F*]. Altogether, these results suggest that *Gpr37l1* deletion leads to sexually dimorphic anxiety-like responses, with female $Gpr37l1^{-/-}$ mice exhibiting increased anxiety-like activity as compared with WT controls.

Discussion

Identifying *GPR37L1* as a contributor to migraine and epilepsy risk

Using an unbiased computational approach, we found that *GPR37L1* coding variants were significantly associated with both epilepsy and migraine supporting their comorbid status and shared etiologies (Rogawski, 2008, 2012; Zarcone and Corbetta, 2017; Shu et al., 2020). Although previously linked to epilepsy (Giddens et al., 2017), the new linkage to migraine in the patient population was both novel and significant for its strong sex bias. The latter may reflect the higher frequency of this diagnosis in the female portion in the DiscovEHR cohort and the population in general, but additional studies will be needed to resolve the connection between sex and GPR37L1 function. To identify the subset of coding variants driving disease associations, we performed bioinformatics and functional analyses to identify variant receptors with altered functional properties. Notably, some variant receptors were indistinguishable from the WT receptor. However, other variant receptors had significantly impacted properties, including those with MISS mutations in critical domains, that is, p.Arg69Trp in the extended N-terminal domain, p.Val361Met at the junction of ICL3 and helix 6, and p.Arg391Cys in the ECL3 loop. Altogether, these results highlight both the need and value for performing integrated computational, bioinformatics, and functional analyses to reveal novel players and pathways for common diseases with multigenic inheritance (Raraigh et al., 2018; Sun and Yu, 2019; Ishikawa et al., 2021).

Support for PSAP as the endogenous ligand

GPR37L1 has been suggested as the receptor for secreted PSAP (Meyer et al., 2013), a neuroprotective protein that has a complex role in lysosomal function (Carvelli et al., 2015). In the lysosome, PSAP is cleaved into four homologous domains, saposins A–D, with each exhibiting distinct regulatory roles in lipid metabolism (Hiraiwa et al., 1993; Leonova et al., 1996). Mutations in the SapC domain cause lysosomal storage diseases, including Gaucher's disease (Kang et al., 2018). However, controversy remains in the assignment of PSAP as the endogenous ligand of GPR37L1. In certain heterologous expression systems, GPR37L1 has been reported to act independently of the TX14(A) agonist (Ngo et al., 2021). However, in KO mouse models, the loss of *Gpr37l1* eliminates prosaptide-evoked signaling in astrocytes (Jolly et al., 2018). Indeed, in SK cells expressing the native GPR37L1, we confirm that WTs respond to both TX14(A) and the native SapC module; KO cells do not respond to TX14(A); and transfection of KO cells with native *GPR37L1* restores the ability of TX14(A) to inhibit cAMP production. Altogether, we have demonstrated that the GPR37L1 receptor can be activated by the SapC module of PSAP and the peptidomimetic TX14(A).

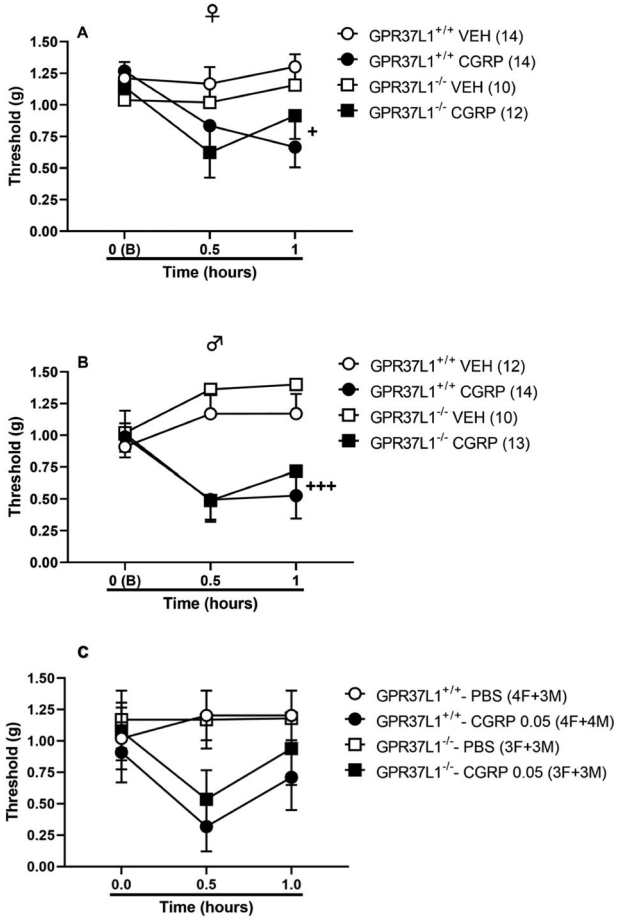

Figure 8. *Gpr37l1* KO (*Gpr37l1*$^{-/-}$) mice show similar responses in an experimental model of migraine. Following acclimation, (***A***) female and (***B***) male *Gpr37l1*$^{-/-}$ and *Gpr37l1*$^{+/+}$ mice were tested for two basal thresholds of periorbital mechanical allodynia using the up-down method and then i.p. injected with calcitonin gene-related peptide (CGRP, 0.1 µg/kg) or VEH. In the CGRP model, both *Gpr37l1*$^{-/-}$ and *Gpr37l1*$^{+/+}$ female and male mice showed reduced thresholds of periorbital mechanical allodynia following CGRP treatment. Data are the mean sensitivity thresholds (grams) ± SEM 10–14 (total mice: 99) mice per group. *$p < 0.05$ difference from *Gpr37l1*$^{+/+}$ groups; $^{+}p < 0.05$, $^{+++}p < 0.001$ difference from VEH-treated groups. ***C***, *Gpr37l1* KO (*Gpr37l1*$^{-/-}$) and WT mice (*Gpr37l1*$^{+/+}$) respond similarly to the CGRP challenge of 0.05 mg/kg dose. Following acclimation, female and male *Gpr37l1*$^{-/-}$ and *Gpr37l1*$^{+/+}$ mice were tested for two basal thresholds of periorbital mechanical allodynia using the up-down method and then i.p. injected with calcitonin gene-related peptide (CGRP, 0.05 mg/kg) or VEH. Thresholds were then recorded at 30 min and 1 h following CGRP or VEH injections. Data are the mean sensitivity thresholds (grams) ± SEM of 6–8 (total mice: 27) mice per group.

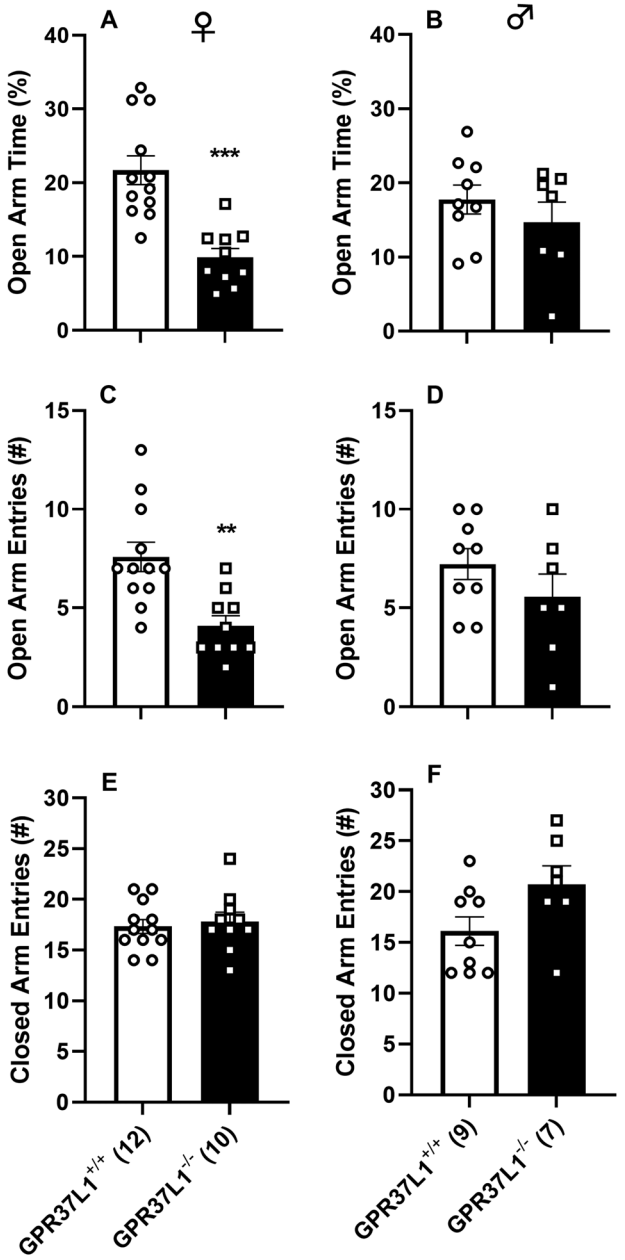

Figure 9. Sex differences in anxiety-like behavior for *Gpr37l1*$^{-/-}$ mice. ***A***, Female but not (***B***) male GPR37L1$^{-/-}$ mice spent less time than *Gpr37l1*$^{+/+}$ mice exploring the open arms of the EPM, a behavior consistent with increased anxiety. Similarly, (***C***) female but not (***D***) male *Gpr37l1*$^{-/-}$ mice showed a reduced number of entries onto the open arms of the maze than *Gpr37l1*$^{+/+}$ mice, a second measure of anxiety-like behavior. ***E,F***, For both sexes, differences in anxiety parameters were accompanied by a similar number of closed arm entries (similar exploration of the EPM maze) for the two phenotypes. Values are presented as mean percent (%) open arm time and mean number of open and closed arm entries ± SEM of 10–12 (female) and 7–9 (male) *Gpr37l1*$^{-/-}$ versus *Gpr37l1*$^{+/+}$ mice. **$p < 0.01$, ***$p < 0.001$ difference between phenotypes.

Dissection of functional differences among GPR37L1 variants

GPR37L1 variants were studied in the null background of *GPR37L1*-KO SK cells, which possess all the regulatory and signaling partners for GPR37L1 function. Previously, inhibition of FSK-induced cAMP production and stimulation of ERK1/2∼P were identified as signaling outputs of GPR37L1 (Meyer et al., 2013; Giddens et al., 2017). Using standard functional assays, we identified differential effects of the rare variants on the two pathways (Table 4). Of particular note, short exposures to TX14(A) induced upregulation of GPR37L1 expression. Although considered atypical for most GPCRs, recent studies has reported that a subset of receptors either maintain or increase signaling in the presence of an agonist, and this ability is crucial for invoking distinct cellular events (Rokosh et al., 1996; Breitwieser, 2012; Morton et al., 2015). Previously, we demonstrated a feed-forward mechanism for the calcium sensing receptor that increases trafficking from an endogenous pool to the cell surface (Grant et al., 2011; Breitwieser, 2012). Further experiments will be needed to sort out the exact mechanism for GPR37L1. Likewise, integrating this insight into models of astrocyte regulation will be critical to understanding the importance of GPR37L1 in the underlying pathologies of migraine and epilepsy.

Identifying cellular role(s) for GPR37L1

The astrocytic role(s) for GPR37L is being investigated. An agnostic RNAi screen for genes involved in cholesterol regulation identified PSAP as a regulator of perinuclear cholesterol levels in astrocytes (Bartz et al., 2009). Recent studies have shown that *Gpr37l1-KO* mice have altered cholesterol homeostasis in astrocytes, which contributes to dysregulation of Patched 1 internalization and trafficking (La Sala et al., 2020). In the current study, KO of *GPR37L1* in SK cells has decreased total cellular cholesterol by ∼20%, which was restored upon transfection with WT *GPR37L1*, suggesting GPR37L1 is a significant contributor for the regulation of total cellular cholesterol. Whether native to the cells or re-expressed in KO SK cells, GPR37L1 increases cellular cholesterol, suggesting the possible presence of an endogenous agonist. PSAP is widely expressed at low levels in most cell types, with low levels of secretion that can be upregulated after stress or injury (Kunihiro et al., 2020). Further, acute stimulation of WT or variant GPR37L1s with TX14(A) differentially upregulated total cellular cholesterol, implicating GPR37L1 in the potential cholesterol cross talk between astrocytes and neurons.

Upregulation of cellular cholesterol levels in response to acute stimulation of GPCRs has not been broadly studied, although a recent report has suggested that NPY stimulates cholesterol synthesis via the SREBP2-HMGCR pathway in mouse hepatocytes (Chen et al., 2020). Specifically, significant upregulation of pathway proteins was observed within an hour, proteins remained elevated for up to 24 h, and cholesterol responses were sensitive to the MEK1/2 inhibitor U0126. Collectively, these results are consistent with GPR37l1 regulation of acute cholesterol changes via a MAPK pathway in SK cells, that is, the ability of GPR37L1 variants to increase ERK1/2 phosphorylation is correlated with upregulation of cell cholesterol in response to TX14(A), and the MEK1/2 inhibitor U0126 significantly attenuates acute cholesterol upregulation by TX14(A).

Assessing in vivo role(s) for GPR37L1

There are both common and rare forms of migraine, and human and mouse studies have begun to reveal the underlying mechanisms that account for the heterogeneity of this disorder (Gormley et al., 2016; Goadsby et al., 2017; Hansen et al., 2017; Sutherland et al., 2019). One specific mechanism involves dysregulation of glutamate homeostasis, including a protective role in astrocytes to counteract the effects of such dysregulation (Capuani et al., 2016; Conti and Pietrobon, 2023). Based on human clinical data, astrocyte localization, and functional studies, we posit a role for GPR37L1 signaling in astrocytes or glial cells. Consistently, dysfunction of brain astrocytes, cells that express the Gpr37l1 receptor, has been shown to trigger migraine-like symptoms in mice (Romanos et al., 2020). In mice, a single systemic administration of CGRP induces periorbital mechanical allodynia and other responses consistent with migraine including spontaneous pain, altered light sensitivity (photophobia), and anxiety-like behavior (Mason et al., 2017; Rea et al., 2018; Sturaro et al., 2023). We examined here the impact of genetic disruption of the *Gpr37l1* receptor and found that its deletion did not affect the ability of an acute CGRP injection to elicit cephalic allodynia. Nevertheless, migraine is a complex disorder that extends beyond acute, episodic pain and involves functional and structural brain changes as well as increased responsiveness (sensitization) of central neurons responsible for pain (Brennan and Peitrobon, 2018; Mungoven et al., 2021). The impact of Gpr37l1 may be increased in chronic migraine, as it has been noted that Gpr37l1 is upregulated in microglia and astrocytes after nerve injury, which may be a compensatory mechanism (Kunihiro et al., 2020), and it is conceivable that the lack of GPR37L1 receptor may affect chronic migraine-like states more than episodic migraine evoked by acute challenge of migraine-provoking substances. Additionally, recent evidence, showing high GPR37L1 receptor expression in satellite glial cells of the human trigeminal ganglia (Yang et al., 2022), has suggested possible protection by GPR37L1 from peripheral sensitization mechanisms, which may also be initiated and maintained by the actions of CGRP. In future experiments, we will examine the role of the GPR37L1 receptor in chronic migraine models leading to sensitization of pain responses (Sturaro et al., 2023). Because comorbidities such as anxiety are frequent in chronic migraineurs and anxiety is a predisposing factor for migraine chronification in humans (Eigenbrodt et al., 2021), we also tested the WT and KO mice in the EPM. Intriguingly, female KO mice exhibited a sex-specific change in anxiety-like behavior, suggesting a possible linkage with chronic migraine.

In conclusion, the current studies have begun by using an unbiased approach to identify a strong association between GPR37L1 rare variants and two comorbid conditions, migraine and epilepsy. In vitro studies revealed that GPR37L1 variants exhibited altered signaling outputs, highlighting potential contributions to clinical phenotypes. Subsequent in vivo studies in KO mice simulating LOF showed a sex bias for females in an anxiety-related trait, though no effect in an acute migraine model. Computational methods in human databases demonstrated a clear connection between GPR37L1 and migraine. Although KO mice did not demonstrate an acute migraine phenotype, receptor KO could induce a chronic migraine phenotype, affect the dose of migraine initiator, or only affect certain types of migraine initiation. Future experiments examining these parameters and studying knock-in mice with humanized GPR37L1 mutants should lead to a better understanding of the role of GPR37L1 mutations in migraine and ultimately help patients.

References

Abul-Husn NS, et al. (2016) Genetic identification of familial hypercholesterolemia within a single U.S. health care system. Science 354:aaf7000.

Bartz F, et al. (2009) Identification of cholesterol-regulating genes by targeted RNAi screening. Cell Metab 10:63–75.

Bonafede M, Sapra S, Shah N, Tepper S, Cappell K, Desai P (2018) Direct and indirect healthcare resource utilization and costs among migraine patients in the United States. Headache 58:700–714.

Breitwieser GE (2012) Minireview: the intimate link between calcium sensing receptor trafficking and signaling: implications for disorders of calcium homeostasis. Mol Endocrinol 26:1483–1495.

Brennan KC, Peitrobon D (2018) A systems neuroscience approach to migraine. Neuron 7:1004–1021.

Burch RC, Loder S, Loder E, Smitherman TS (2015) The prevalence and burden of migraine and severe headache in the United States: updated statistics from government health surveillance studies. Headache 55:21–34.

Capuani C, Melone M, Tottene A, Bragina L, Crivellaro G, Santello M, Casari G, Conti F, Pietrobon D (2016) Defective glutamate and K+ clearance by astrocytes in familial hemiplegic migraine type 2. EMBO Mol Med 8:967–986.

Carey DJ, Fetterolf SN, Davis FD, Faucett WA, Kirchner HL, Mirshahi LI, Murray MF, Smelser DT, Gerhard GS, Ledbetter DH (2016) The Geisinger MyCode Community Health Initiative: an electronic health record-linked biobank for precision medicine research. Genet Med 18:906–913.

Carvelli L, Libin Y, Morales CR (2015) Prosaposin: a protein with differential sorting and multiple functions. Histol Histopathol 30:647–660.

Chen F, Zhou Y, Shen M, Wang Y (2020) NPY stimulates cholesterol synthesis by activating the SREBP2-HMGCR pathway through the Y1 and Y5 receptors in murine hepatocytes. Life Sci 262:118478.

Coleman JLJ, et al. (2018) Orphan receptor GPR37L1 contributes to the sexual dimorphism of central cardiovascular control. Biol Sex Differ 9:14.

Coleman JLJ, Ngo T, Schmidt J, Mrad N, Liew CK, Jones NM, Graham RM, Smith NJ (2016) Metalloprotease cleavage of the N terminus of the orphan G protein-coupled receptor GPR37L1 reduces its constitutive activity. Sci Signal 9:ra36.

Coleman JLJ, Ngo T, Smythe RE, Cleave AJ, Jones NM, Graham RM, Smith NJ (2020) The N-terminus of GPR37L1 is proteolytically processed by matrix metalloproteases. Sci Rep 10:19995.

Conti F, Pietrobon D (2023) Astrocytic glutamate transporters and migraine. Neurochem Res 48:1167–1179.

Dershem R, Metpally RPR, Jeffreys K, Krishnamurthy S, Smelse DT, Hershfinkel M, Regeneron Genetics Center, Carey DJ, Robishaw JD, Breitwieser GE (2019) Rare variant pathogenicity triage and inclusion of synonymous variants improves analysis of disease associations. J Biol Chem 294:18109–18121.

Dewey FE, et al. (2016) Distribution and clinical impact of functional variants in 50,726 whole-exome sequences from the DiscovEHR cohort. Science 354:aaf6814.

Eigenbrodt AK, et al. (2021) Diagnosis and management of migraine in ten steps. Nat Rev Neurol 17:501–514.

Fricker L, Devi LA (2018) Orphan neuropeptides and receptors: novel therapeutic targets. Pharmacol Ther 185:26–33.

Gawlak D, Euniewska J, Stojak W, Hovhannisyan A, Strozynska A, Manka-Malara K, Adamiec M, Rysz A (2017) The prevalence of orodental trauma during epileptic seizures in terms of dental treatment: survey study. Neurol Neurochir Pol 51:361–365.

Giddens MM, et al. (2017) GPR37L1 modulates seizure susceptibility: evidence from mouse studies and analyses of a human GPR37L1 variant. Neurobiol Dis 106:181–190.

Goadsby PJ, Holland PR, Martins-Oliveira M, Hoffmann J, Schankin C, Akerman S (2017) Pathophysiology of migraine: a disorder of sensory processing. Physiol Rev 97:553–622.

Gormley P, et al. (2016) Meta-analysis of 375,000 individuals identifies 38 susceptibility loci for migraine. Nat Genet 48:856–866.

Grant MP, Stepanchick A, Cavanaugh A, Breitwieser GE (2011) Agonist-driven maturation and plasma membrane insertion of calcium-sensing receptors dynamically controls signal amplitude. Sci Signal 4:ra78.

Hanin A, et al. (2021) Disturbances of brain cholesterol metabolism: a new excitotoxic process associated with status epilepticus. Neurobiol Dis 154:105346.

Hansen RD, Christensen AF, Olesen J (2017) Family studies to find rare high risk variants in migraine. J Headache Pain 18:32.

Hiraiwa M, O'Brien JS, Kishimoto Y, Galdzicka M, Fluharty AL, Ginns EI, Martin BM (1993) Isolation, characterization, and proteolysis of human prosaposin, the precursor of saposins (sphingolipid activator proteins). Arch Biochem Biophys 304:110–116.

Huang Y, Xiao H, Qin X, Nong Y, Zou D, Wu Y (2017) The genetic relationship between epilepsy and hemiplegic migraine. Neuropsychiatr Dis Treat 13:1175–1179.

Ishikawa T, et al. (2021) Functionally validating SCN5A variants allow interpretation of pathogenicity and prediction of lethal events in Brugada syndrome. Eur Heart J 42:2854–2863.

Jolly S, Bazargani N, Quiroga AC, Prongle NP, Attwell D, Richardson WD, Li H (2018) G protein-coupled receptor 37-like 1 modulates astrocyte glutamate transporters and neuronal NMDA receptors and in neuroprotective in ischemia. Glia 66:47–61.

Kang L, Zhan X, Ye J, Han L, Qiu W, Gu X, Zhang H (2018) A rare form of Gaucher disease resulting from saposin C deficiency. Blood Cells Mol Dis 68:60–65.

Kunihiro J, et al. (2020) Prosaposin and its receptors GRP37 and GPR37L1 show increased immunoreactivity in the facial nucleus following facial nerve transection. PLoS One 15:e0241315.

La Sala G, Di Pietro C, Matteoni R, Bolasco G, Marazziti D, Tocchino-Valentini GP (2020) Gpr37l1/prosaposin receptor regulates Ptch1 trafficking, Shh production, and cell proliferation in cerebellar primary astrocytes. J Neurosci Res, Epub ahead of print.

Leonova T, Qi X, Bencosme A, Ponce E, Sun Y, Grabowski GA (1996) Proteolytic processing patterns of prosaposin in insect and mammalian cells. J Biol Chem 271:17312–17320.

Liu B, Mosienko V, Vaccari Cardoso B, Prokudina D, Huentelman M, Teschemacher AG, Kasparov S (2018) Glio-and neuro-protection by prosaposin is mediated by orphan G-protein coupled receptors GPR37L1 and GPR37. Glia 66:2414–2426.

Manolio TA, et al. (2009) Finding the missing heritability of complex diseases. Nature 461:747–753.

Mashiko D, Fujihara Y, Satouh Y, Miyata H, Isotani A, Ikawa M (2013) Generation of mutant mice by pronuclear injection of circular plasmid expressing Cas9 and single guided RNA. Sci Rep 3:3355.

Mason BN, Kaiser EA, Kuburas A, Loomis MM, Latham JA, Garcia-Martinez LF, Russo AF (2017) Induction of migraine-like photophobic behavior in mice by both peripheral and central CGRP mechanisms. J Neurosci 37: 204–216.

Meyer RC, Giddens MM, Schaefer SA, Hall RA (2013) GPR37 and GPR37L1 are receptor for the neuroprotective and glioprotective factors prosaptide and prosaposin. Proc Natl Acad Sci U S A 110:9529–9523.

Min KD, et al. (2010) Identification of genes related to heart failure using global gene expression profiling of human failing myocardium. Biochem Biophys Res Commun 393:55–60.

Morton RA, Baptista-Hon DT, Hales TG, Lovinger DM (2015) Agonist- and antagonist-induced up-regulation of surface 5-HT3 a receptors. Br J Pharmacol 172:4066–4077.

Mouat MA, Coleman JLJ, Wu J, Dos Remedios CG, Feneley MP, Graham RM, Smith NJ (2021a) Involvement of GPR37L1 in murine blood pressure regulation and human cardiac disease pathophysiology. Am J Physiol Heart Circ Physiol 321:H807–H817.

Mouat MA, Jackson KL, Coleman JLJ, Paterson MR, Graham RM, Head GA, Smith NJ (2021b) Deletion of orphan G protein-coupled receptor GPR37L1 in mice alters cardiovascular homeostasis in a sex-specific manner. Front Pharmacol 11:600266.

Mulder EJ, et al. (2003) Genetic and environmental influences on migraine: a twin study across six countries. Twin Res 6:422–431.

Mungoven TJ, Henderson LA, Meylakh N (2021) Chronic migraine pathophysiology and treatment: a review of current perspectives. Front Pain Res 2:705276.

Ngo T, Wilkins BP, So SS, Keov P, Chahal KK, Finch AM, Coleman JLJ, Kufareva I, Smith NJ (2021) Orphan receptor GPR37L1 remains unliganded. Nat Chem Biol 17:383–386.

Noseda R, Burstein R (2013) Migraine pathophysiology: anatomy of the trigeminovascular pathway and associated neurological symptoms, CSD, sensitization and modulation of pain. Pain 154:Suppl 1:S44–53.

Omasits U, Ahrens CH, Muller S, Wollscheid B (2014) Protter: interactive protein feature visualization and integration with experimental proteomic data. Bioinformatics 30:884–886.

Raraigh KS, et al. (2018) Functional assays are essential for interpretation of missense variants associated with variable expressivity. Am J Hum Genet 102:1062–1077.

Rea BJ, et al. (2018) Peripherally administered calcitonin gene-related peptide induces spontaneous pain in mice: implications for migraine. Pain 159: 2306–2317.

Rogawski MA (2008) Common pathophysiologic mechanisms in migraine and epilepsy. Arch Neurol 65:709–714.

Rogawski MA (2012) Migraine and epilepsy-shared mechanisms within the family of episodic disorders. In: *Jasper's basic mechanisms of the epilepsies (internet)*, Ed 4, (Noebels JL, Avoli M, Rogawski MA, Olsen RW, Delgado-Escueta AV, eds). Bethesda (MD): National Center for Biotechnology Information (US).

Rokosh DG, Stewart AF, Chang KC, Bailey BA, Karliner JS, Camacho SA, Long CS, Simpson PC (1996) Alpha1-adrenergic receptor subtype mRNAs are differentially regulated by alpha1-adrenergic and other hypertrophic stimuli in cardiac myocytes in culture and in vivo. J Biol Chem 271:5839–5843.

Romanos J, Benke D, Pietrobon D, Zeilhofer HU, Santello M (2020) Astrocyte dysfunction increases cortical dendritic excitability and promotes cranial pain in familial migraine. Sci Adv 6:eaaz1584.

Russell MB, Iselius L, Olesen J (1995) Inheritance of migraine investigated by complex segregation analysis. Hum Genet 96:726–730.

Shu Y, Xu Y, Xiao W, Deng X, Zeng Y, Chen R, Xiao B, Long H (2020) A conjoint analysis of epilepsy and migraine through network-and-pathway-based method. Ann Palliat Med 9:2642–2653.

Sturaro C, Fakhoury B, Targowska-Duda KM, Zribi G, Schoch J, Ruzza C, Calo G, Toll L, Cippitelli A (2023) Preclinical effects of cannabidiol in an experimental model of migraine. Pain 164:2540–2552.

Sun H, Yu G (2019) New insights into the pathogenicity of non-synonymous variants through multi-level analysis. Sci Rep 9:1667.

Sutherland HG, Albury CL, Griffiths LR (2019) Advances in genetics of migraine. J Headache Pain 20:72.

Sutherland HG, Maksemous N, Albury CL, Ibrahim O, Smith RA, Lee RA, Haupt LM, Jenkins B, Tsang B, Griffiths LR (2020) Comprehensive exonic sequencing of hemiplagic migraine-related genes in a cohort of suspected probands identifies known and potential pathogenic variants. Cells 9:2368.

Tang XL, Wang Y, Li D, Luo J, Liu MY (2012) Orphan G protein-coupled receptors (GPCRs): biological functions and potential drug targets. Acta Pharmacol Sin 33:363–371.

Tardiolo G, Bramanti P, Mazzon E (2019) Migraine: experimental models and novel therapeutic approaches. Int J Mol Sci 20:2932.

Targowska-Duda KM, et al. (2020) NOP receptor agonist attenuates nitroglycerin-induced migraine-like symptoms in mice. Neuropharmacology 170:108029.

Yang L, et al. (2022) Human and mouse trigeminal ganglia cell atlas implicates multiple cell types in migraine. Neuron 110:1806–1821.

Zarcone D, Corbetta S (2017) Shared mechanisms of epilepsy, migraine and affective disorders. Neurol Sci 38:73–76.

Zheng X, Asico LD, Ma X, Konkalmatt PR (2019) G protein-coupled receptor 37L1 regulates nal sodium transport and blood pressure. Am J Physiol Renal Physiol 316:F506–F516.